

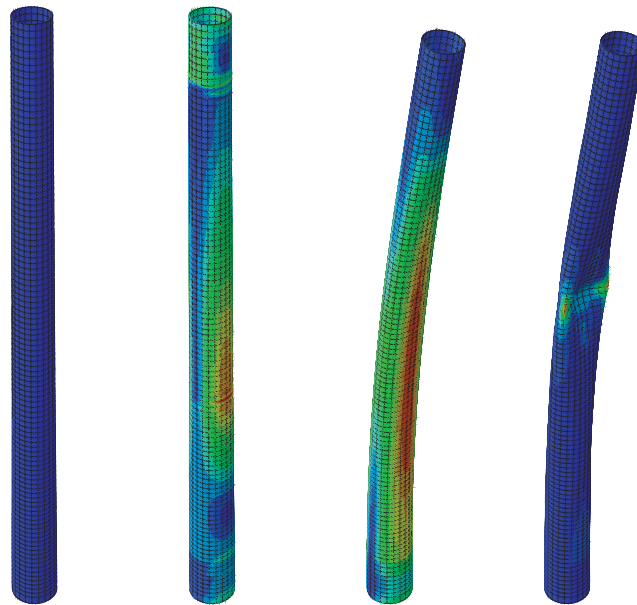
AALBORG UNIVERSITY  
SCHOOL OF ENGINEERING AND SCIENCE  
MASTER THESIS IN STRUCTURAL AND CIVIL ENGINEERING

---

# NONLINEAR NUMERICAL ANALYSIS OF A DYNAMICALLY LOADED WIND TURBINE TOWER

---

June 10, 2014



Christian Munk Svendsen - 20093319  
csvend09@student.aau.dk  
Rasmus Bøgelund Madsen - 20093323  
rbma09@student.aau.dk



**School of Engineering and Science**

Aalborg University  
Sohngårdsholmsvej 57  
9000 Aalborg

Title:

Nonlinear numerical analysis of a  
dynamically loaded wind turbine  
tower

Project period:

4th semester, 2014  
02-01-2014 to 06-10-2014

Students:

Christian Munk Svendsen  
20093319  
Rasmus Bøgelund Madsen  
20093323

Supervisors:

Lars Vabbersgaard Andersen  
Søren Madsen

Printed editions: 5

Number of pages: 79 + CD

Abstract:

This thesis depicts the effects and consequences of simplifying time-varying loads to equivalent static loads acting on a finite element modelled wind turbine tower. The structural response is assessed with respect to structural stability behaviour. Limit load buckling, inertia effects, and geometrical nonlinearities are central topics in this thesis. The limit load buckling behaviour of a simple truss under static and time-varying loads is presented at first, and findings are used for further analysis of a wind turbine tower. The analysis of a wind turbine tower is initiated with an examination of the structural response with different simple time-varying load types and combinations. Combinations of real wind loads are applied to the tower, and relations between load magnitude and duration are found.

---

Christian Munk Svendsen      Rasmus Bøgelund Madsen



---

# Preface

---

This Master's thesis is made by Christian Munk Svendsen and Rasmus Bøgelund Madsen during the 4th semester on the M.Sc. in Structural and Civil Engineering at Aalborg University. The thesis is written in the period between 1st of February and 10th of June 2014.

## **Reading guide**

Through the report, sources are referred to by surname of author and year of publication, i.e. [Surname, year]. All the sources will be shown in the bibliography in the end of the report. If a source has more than two authors, only the first will be mentioned by name, while the remaining authors are referred as "et al."

In the bibliography books will be listed by author, title, and publisher. Web pages are listed by author and URL address. Sources on figures, pictures, and tables will be displayed in the caption below. Figures and tables will be numbered by given chapter, i.e. the first figures in e.g. chapter 3, will be figure 3.1, figure 3.2 etc.

Project plan and syllabus are included as appendix. A CD is enclosed and contains the digital appendix with relevant Abaqus files, Matlab codes, wind data, and wind loads.



---

# Contents

---

<b>1</b>	<b>Introduction</b>	<b>1</b>
1.1	The concept of instability . . . . .	1
1.2	State-of-the-art . . . . .	3
1.3	Thesis statement . . . . .	4
<b>2</b>	<b>Limit Load Buckling of Simple Truss</b>	<b>5</b>
2.1	Static analysis . . . . .	7
2.2	Dynamic analysis . . . . .	8
<b>3</b>	<b>Modelling of Wind Turbine Tower</b>	<b>15</b>
3.1	Tower properties and boundary conditions . . . . .	15
3.2	Inertia considerations . . . . .	17
3.3	Finite element modelling . . . . .	20
3.4	Convergence analysis . . . . .	22
<b>4</b>	<b>Analysis with Simple Time-varying Loads</b>	<b>25</b>
4.1	Impulse loading . . . . .	27
4.2	Ramped loading . . . . .	31
4.3	Harmonic loading . . . . .	32
4.4	Damping of structural response . . . . .	33
4.5	Imperfection sensitivity analysis . . . . .	37
<b>5</b>	<b>Analysis with Combined Time-varying Wind Loads</b>	<b>43</b>
5.1	Simple load combinations . . . . .	43
5.2	Wind generated loads . . . . .	45
<b>6</b>	<b>Conclusion</b>	<b>53</b>
	<b>Bibliography</b>	<b>55</b>
<b>A</b>	<b>Simple model</b>	
<b>B</b>	<b>Tower properties</b>	
B.1	Tower dimensions . . . . .	59
<b>C</b>	<b>Nonlinear iteration methods</b>	
C.1	Newton-Rhapson method . . . . .	61
C.2	Modified Newton-Rhapson method . . . . .	62

- C.3 Arc-length method . . . . . 62
- D Imperfection mode shapes**
- E Wind generated loads**

# CHAPTER 1

---

## Introduction

---

The global wind power industry is rapidly growing due to the increasing demand of renewable energy. More than 238 GW of wind power was installed worldwide by the end of 2011, and 70% of this capacity was added between 2007 and 2011. The World Wind Energy Association has predicted, that the global wind power capacity will reach 1500GW by the year 2020 [Sahu et al., 2013]. The growth in the wind power industry and competition on the global market requires development and optimization of the structural design of wind turbines.

One of the biggest structural parts of a wind turbine is the wind turbine tower, which has to transfer loads from wind and heavy structural parts to the foundation. These relatively slender cylindrical steel towers have reached heights up to 140m, which requires a correspondingly large amount of steel [Vestas Wind Systems A/S, 2014]. Research and development of the entire design phase of such structures would lead to better understanding and prediction of the structural behaviour and might lead to a reduction of construction costs.

All types of possible failures must be taken into account when designing the tower. This is, according to Eurocode, ensured with the limit state design method. This method is divided into ultimate limit state and serviceability limit state. Ultimate limit state consists of plastic limit state, stability limit state, and fatigue limit state [DS/EN 1990, 2007]. Instability is a fundamental phenomenon of slender structures, and is considered as the design parameter in this thesis.

### 1.1 The concept of instability

The study of stability is applied in many fields of engineering. Instability problems are common in slender structures subjected to compression, such as columns, silos, thin-walled towers, and shell structures. The structure will at some load undergo big lateral deformations with reduced load bearing capacity or a total collapse. This is known as buckling, see Figure 1.1.



**Figure 1.1.** Dramatic collapse of a wind turbine tower at a wind energy facility, Arlington, Wyoming, [Brome, 2010]

### 1.1.1 Buckling of slender structures

Instability of structures is divided into limit load buckling and bifurcation buckling. Limit load buckling happens, when the load has reached a level, where the structure must undergo large deformations in order to retain equilibrium between internal and external forces. This dynamic jump is often referred to as snap-through [ECCS Technical Committee 8, 2008]. The load-displacement relation for limit load buckling is illustrated in Figure 1.2.

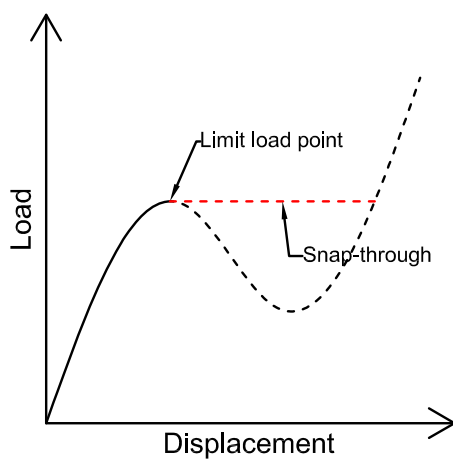


**Figure 1.2.** Load-displacement curve for limit load buckling.

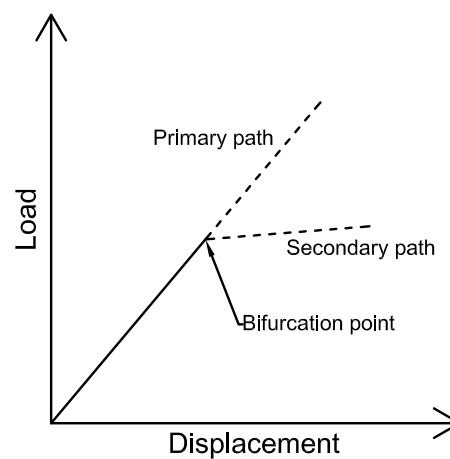


**Figure 1.3.** Load-displacement curve for bifurcation buckling.

Linear bifurcation buckling happens, when there are two or more ways, the structure can be in equilibrium, see Figure 1.3. The structure follows a primary path in the beginning and will reach a bifurcation point, where the structure can either follow an extension of the primary path, which is unstable, or it can follow a stable secondary path. In reality the structure will always follow the secondary path, where the deformations will follow a new pattern, which either can have post-buckling strength or not. The unstable

primary path after the bifurcation point is only theoretical possible, since real structures always will have a degree of imperfection and load eccentricity. Imperfections may arise during manufacturing process and could cover welding seam, dents, variation in element thickness's, and inhomogeneous material properties.

Bifurcation buckling is solved as an eigenvalue-problem, which is based on the assumption of linear-elastic material behaviour, while limit load buckling often happens with so large deformations that the assumption of linearity becomes inadequate. The linear-elastic relation between displacements and forces gives accurate and sufficient approximations in the most common structural engineering tasks. This assumption of infinitesimal strains is unfortunately not always adequate enough, but provides correct results in many cases. There are different variants of nonlinearity with different approaches, but geometrical nonlinearity is an important factor through-out this thesis. This type of nonlinearity arises when deformations becomes so large that the structural stiffness depends on the deformation itself. Another type of nonlinearity is where material properties depends on the state of stress/strain (hardening, softening) [ECCS Technical Committee 8, 2008] [Cook et al., 2001].

## 1.2 State-of-the-art

Stability of slender structures has been studied for many years, and several theories and design criteria are developed and widely used. An expression, for the maximum compressive load a column can withstand without buckling, was formulated by Leonhard Euler (1707-1783). This expression was based on perfect structural geometry and perfectly linear elastic material assumption [Williams and Todd, 2000]. A solution for the compressive buckling load on a cylindrical shell was found in 1908-1910 by Lorenz and Timoshenko [Schmidt, 2000]. This critical load for shells was very theoretical, and experiments showed, that the actual critical loads were as low as 1/10 of the calculated bifurcation buckling load [Almroth and Brogan, 1972]. A comprehensive study of the effects of imperfections and geometrical nonlinearities of a cylindrical shell was made by Donnel and Wan in 1950. It was one of the first studies that clearly depicted, that differences between experiments and theory of buckling analysis was caused by geometrical imperfections [Bushnell, 1989]. It was found, that the load capacity significantly decreases as function of increasing magnitude of imperfection [Castro et al., 2013]. The reduced load bearing capacity is strongly dependent on the nature and amplitude of the imperfection [ECCS Technical Committee 8, 2008].

The study of shell stability has been ongoing ever since, and the ability to model complicated structures with numerical methods, such as the finite element method, has also contributed to a more or less conclusively understanding of stability problems. However, the same general agreements and findings of stability does not include dynamic instability problems [Schmidt, 2000]. As mentioned, the effects of imperfections have been investigated since the 1950s, and the understanding of imperfections has now reached a high sophisticated level, but this does not include a description of how imperfections affect the structural response in a dynamic analysis [Schmidt, 2000].

Today's finite element programs have the ability to apply various features such as different shell theories, material and geometrical nonlinearities, dynamic analysis, and damping

models. [Simulia, 2011]

The assessment of loads on wind turbines has been developed along with growth in wind power industry and can be extracted from sophisticated aeroelastic models. E.g. the National Renewable Energy Laboratory has developed an aeroelastic simulation tool called FAST, which simulates forces on a wind turbine. [Jonkman et al., 2009]

### 1.3 Thesis statement

In structural design, dynamic loads are often approximated with equivalent static loads. These static loads are often maximum or peak values of load series. But winds are obviously not static, and will not act as static loads on a wind turbine. The influence of time is intuitively easy to comprehend. The structural response to a load acting in 10 seconds is more significant than the response to the same load acting in 1 second.

Simplifications of time-varying loads are made to lower the complexity of structural calculations, but dynamic features of a structure are omitted as a consequence. It is evident to wonder, to which extent these simplifications are valid, and if it is even possible to imitate time-varying loads with static loads. The uncertainty about the transition from dynamic to static loads is the motivation behind this thesis. The aim of this thesis is to answer the following:

- How is the stability of a wind turbine tower affected by simplifying time-varying loads to equivalent static loads, and is it reasonable to use peak values to describe time-varying wind loads?

#### 1.3.1 Project description

This thesis examines the structural response of a wind turbine tower with the presence of different time-varying loads with buckling instability as the assumed design parameter.

A parameter study of the structural response of a simple truss is presented at first. The idea of this study is to examine mechanisms of limit load buckling, inertia affects, and geometrical nonlinearities, and then use this knowledge for further and more advanced calculations of a full-size finite element modelled wind turbine tower, where similar time-varying loads are applied. Structural damping and imperfections will always be present in a real structure. The effects of these are included in a finite element analysis of a wind turbine tower. Finally, real time-varying wind generated loads are analysed and compared to the magnitudes and duration of the more simple loads described earlier.

## CHAPTER 2

# Limit Load Buckling of Simple Truss

The idea of this chapter is to examine how time-varying loads affects the response of a simple two bar truss with a single degree of freedom, which geometry leads to a nonlinear snap-through buckling behaviour. A static analysis forms the basis for a dynamic, where different time-varying load types are applied. A brief section with remarks will discuss and identify findings and results. This knowledge are then used for further finite element analysis of a wind turbine tower.

The snap-through phenomenon is illustrated by a simply supported truss, consisting of two bars with cross-section area  $A$ , elastic modulus  $E$ , and axial force denoted  $N$  as shown in Figure 2.1.

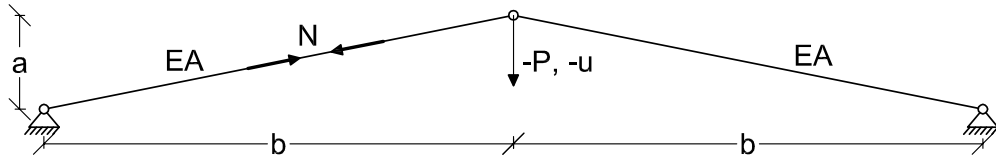


**Figure 2.1.** Simply supported truss with two bar elements. A vertical load downward load,  $-P$ , is applied in the middle top node which leads to the vertical nodal displacement,  $-u$ . The displacement,  $u$ , is zero at the initial configuration of the structure. [Krenk, 2009]

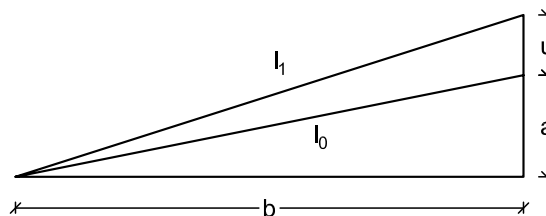


**Figure 2.2.** Definition of initial bar length,  $l_0$ , and current bar length,  $l_1$ .

The initial and current length  $l_0$  and  $l_1$  are seen in Figure 2.2 and given as:

$$l_0 = \sqrt{b^2 + a^2} \simeq b \left( 1 + \frac{1}{2} \frac{a^2}{b^2} \right) \quad (2.1)$$

$$l_1 = \sqrt{b^2 + (a + u)^2} \simeq b \left( 1 + \frac{1}{2} \left( \frac{a + u}{b} \right)^2 \right) \quad (2.2)$$

Which are only applicable when the geometry of the truss implies that  $a \ll b$ . Strains are defined as:

$$\varepsilon = \frac{l_1 - l_0}{l_0} \simeq \frac{a}{l_0} \frac{u}{l_0} + \frac{1}{2} \left( \frac{u}{l_0} \right)^2 \quad (2.3)$$

The nonlinear relation between displacement and load is obtained by equilibrium in the node:

$$P = 2 \frac{a + u}{l_1} N \simeq \frac{2EA}{l_0^3} \left( au + \frac{1}{2} u^2 \right) (a + u) \quad (2.4)$$

The nonlinear expression in Equation 2.4 is normalized and plotted in Figure 2.3, and the corresponding deformed states of the structure are shown in Figure 2.4.

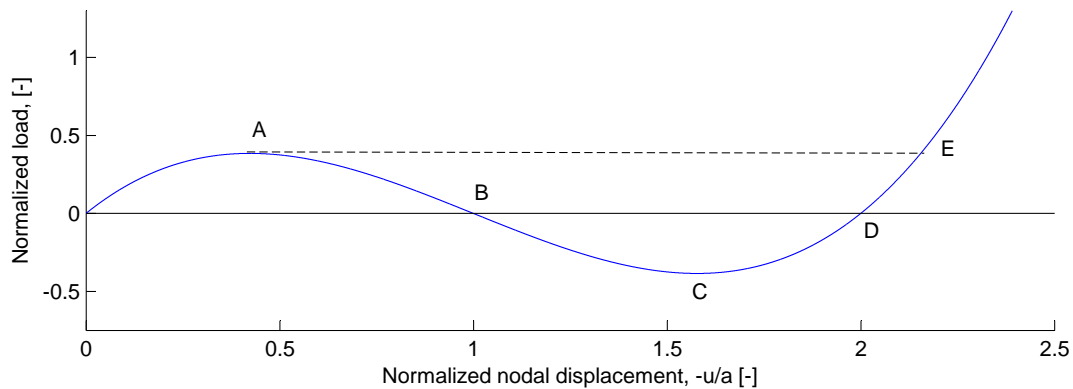


**Figure 2.3.** Normalized load-displacement curve. Normalized load on y-axis values are  $\frac{-P}{EA} \left( \frac{l_0}{a} \right)^3$ .

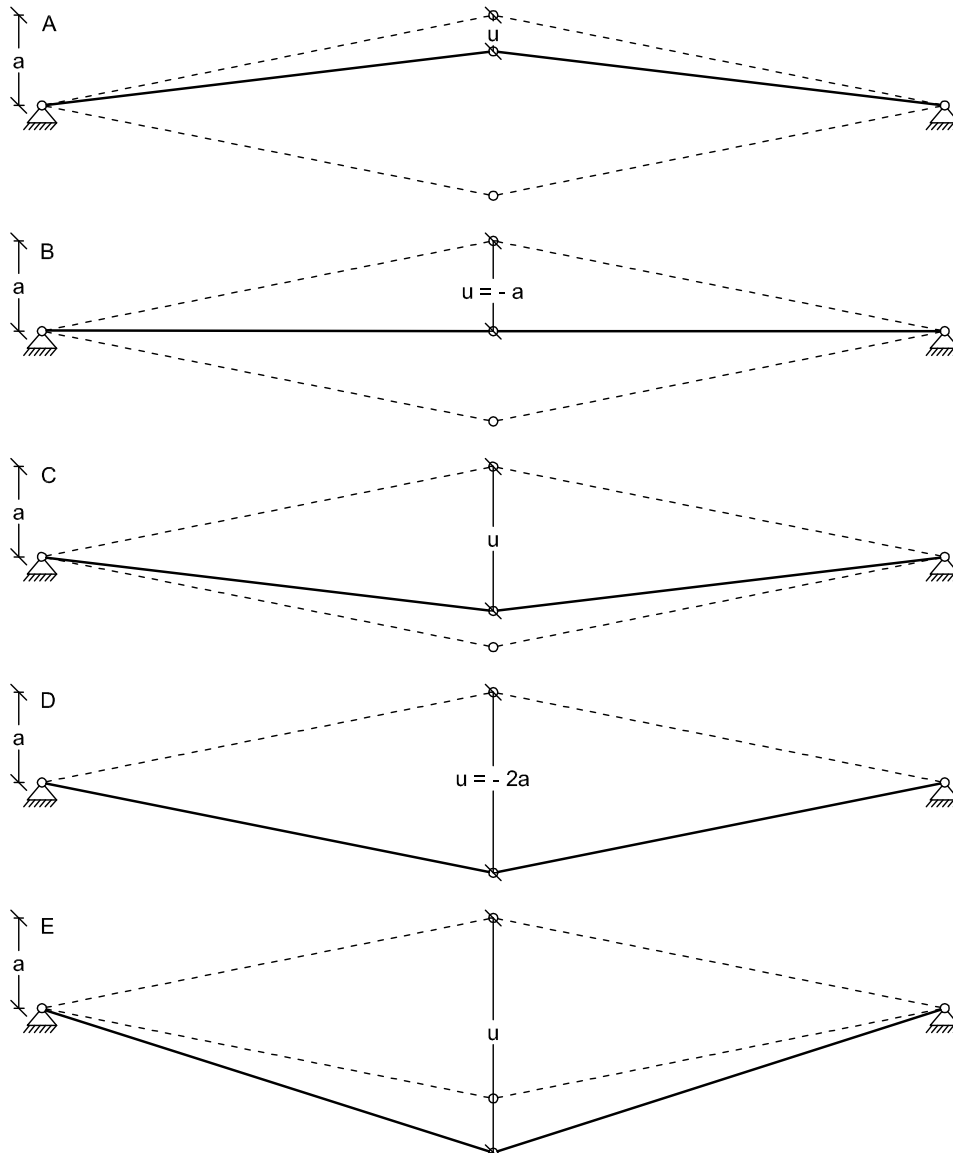


**Figure 2.4.** Deformed shapes of the truss. Dashed lines indicate initial and inverted undeformed states.

As seen in Figure 2.3, a downward load  $-P$  leads to a local maximum  $A$ . An additional increase in load, forces a snap-through motion with large deformations of the structure (dashed line from point  $A$  to  $E$ ). This happens in order to obtain equilibrium between internal bar forces and the external applied load. The axial compressive bar forces reaches a maximum in point  $B$ , and the inverted initial structural geometry appears at point  $D$ . [ECCS Technical Committee 8, 2008] [Krenk, 2009]

## 2.1 Static analysis

A static analysis of the truss is performed based on arbitrarily assumed geometry and material properties listed in Table 2.1. It is though ensured that  $a \ll b$ , which is a requirement when using Equation 2.4.

Height, $a$	2 [m]
Width, $b$	10 [m]
Cross-section, $A$	0.01 [m <sup>2</sup> ]
Elastic modulus, $E$	$200 \cdot 10^9$ [Pa]

**Table 2.1.** Structural geometry and material properties.

The load-displacement curve is plotted to the left in Figure 2.5, and the axial bar force to the right.

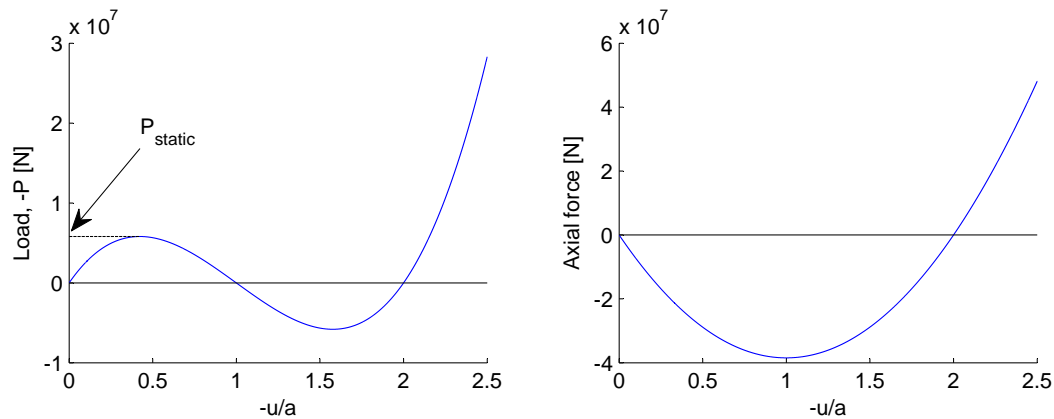


**Figure 2.5.** Load-displacement curve to the left and axial bar force to the right.

The limit load  $P_{static}$  is calculated to  $-5.807 \cdot 10^3$  kN, which corresponds to a displacement of  $-0.84$  m.  $P_{static}$  is used as a reference load for further dynamic calculations.

## 2.2 Dynamic analysis

Time-varying loads are applied in order to examine the dynamic response of the system and their influence on the snap-through behaviour. A lumped mass is added at the middle node. Additional properties are given in Table 2.2. Geometry and material properties are unchanged.

Lumped mass, $m$	$1 \cdot 10^7$ [kg]
1st natural frequency, $\omega_0$	1.23 [rad/s]
1st natural period, $T_0$	5.11 [s]

**Table 2.2.** Additional properties used in dynamic analysis. The natural frequency is calculated from the initial undeformed configuration. Calculations can be seen in Appendix A.

Three different time-varying load scenarios are applied to the system:

- **Impulse load**, Figure 2.6 (a):

A load with constant magnitude are applied and removed instantaneously. Load duration is denoted  $t_{impulse}$ .

- **Ramped load**, Figure 2.6 (b):  
A ramped load is applied and instantaneously removed. Load duration is denoted  $t_{ramp}$ .
- **Harmonic load**, Figure 2.6 (c):  
The load is applied as a sinusoid with no change in load direction. The load period is denoted  $T_{harmonic}$ .

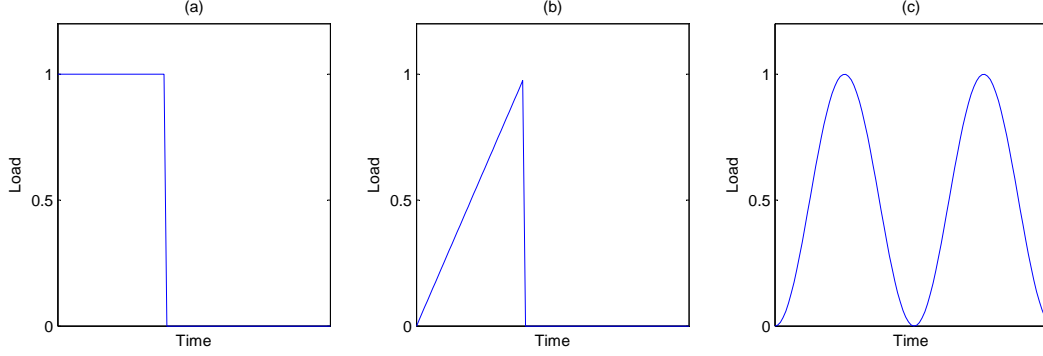


**Figure 2.6.** The three different time-varying load types.

The magnitude of the load is expressed as a ratio between applied load and static limit load:

$$load\ ratio = \frac{P}{P_{static}} \quad (2.5)$$

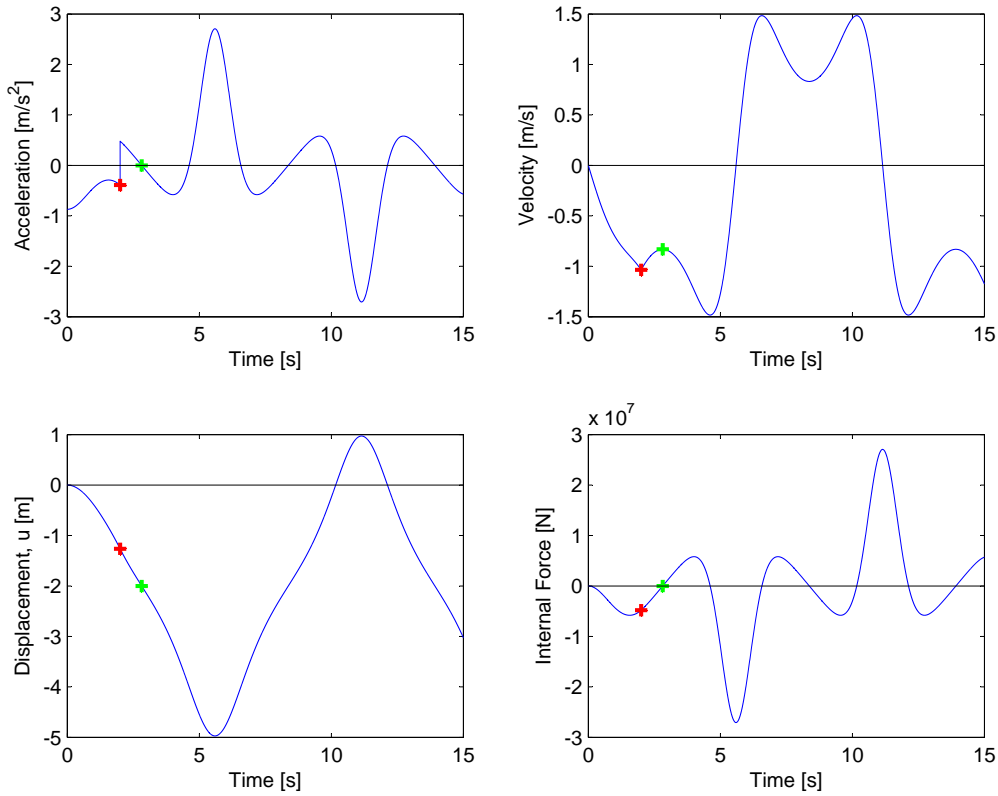
The load accelerates the mass, and internal forces are build up until the residual force,  $R(u)$ , becomes zero. The internal force is related to each time-dependent displacement increment as in Equation 2.4, which leads to:

$$R(u(t)) = F_{ext} - F_{int}(u(t)) \simeq F_{ext} - \frac{2EA}{l_0^3} \left( au(t) + \frac{1}{2}u(t)^2 \right) (a + u(t)) \quad (2.6)$$

An initial acceleration of the mass is found as the external force divided by the lumped mass. Velocity and displacement of the mass are then calculated by simple explicit time integration. Each displacement yields a change in residual force, which gives a new acceleration and so on. The integration scheme can be found in Digital Appendix `simpletruss.m`. The system is assumed to be undamped in all three load scenarios.

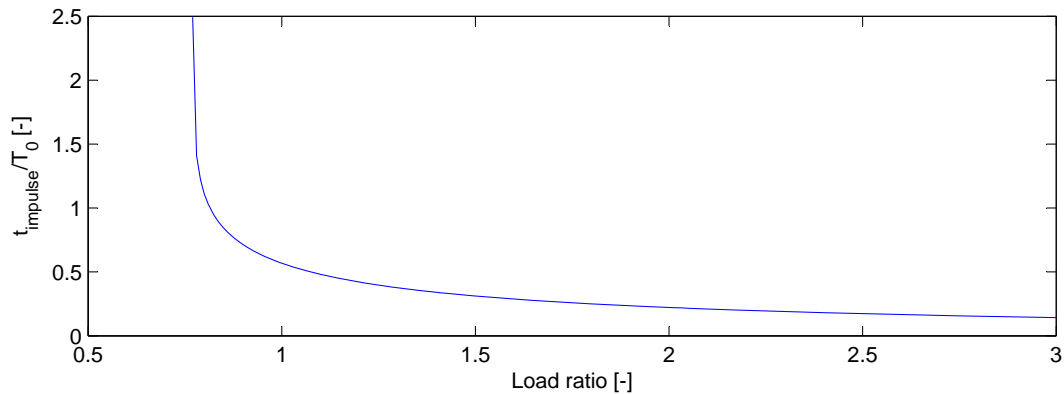
### 2.2.1 Impulse loading

Figure 2.7 shows the acceleration, velocity, displacement, and internal force as a function of time. The load in this example is applied long enough to trigger snap-through (red dots), and the snap-through happens a bit later (green dot).



**Figure 2.7.** Structural response to an impulse load with load ratio 1.5, and  $t_{impulse}=2s$ . Snap through happens after approximately 2.8 seconds.

It should be mentioned, that the snap-through does not happen instantaneously as in the static case but more as a smooth motion. This is caused by inertia effects, where movement of mass is a time-dependent process. It is assumed, that the structure has snapped through when  $u < -a$  (after point B in Figure 2.3). The duration,  $t_{impulse}$ , that is necessary to cause snap-through, is found for several load ratios. The normalized relation between load duration and load is seen in Figure 2.8.



**Figure 2.8.** Ratio between impulse load duration  $t_{impulse}$  and natural period  $T_0$ , as function of load ratios.

It is evident, that it is possible for a load ratio below one to cause snap-through, given

that  $t_{impulse}$  is sufficiently large. It turns out, that the same asymptotic relation exists when different lumped masses are applied to the system. An increase in mass would result in a higher natural period with corresponding bigger load duration needed to cause snap-through and vice versa. The mass is now varying, and the ratio  $\frac{t_{impulse}}{T_0}$  is plotted as function of  $T_0$  in Figure 2.9. The load ratio is kept constant at 1.5.

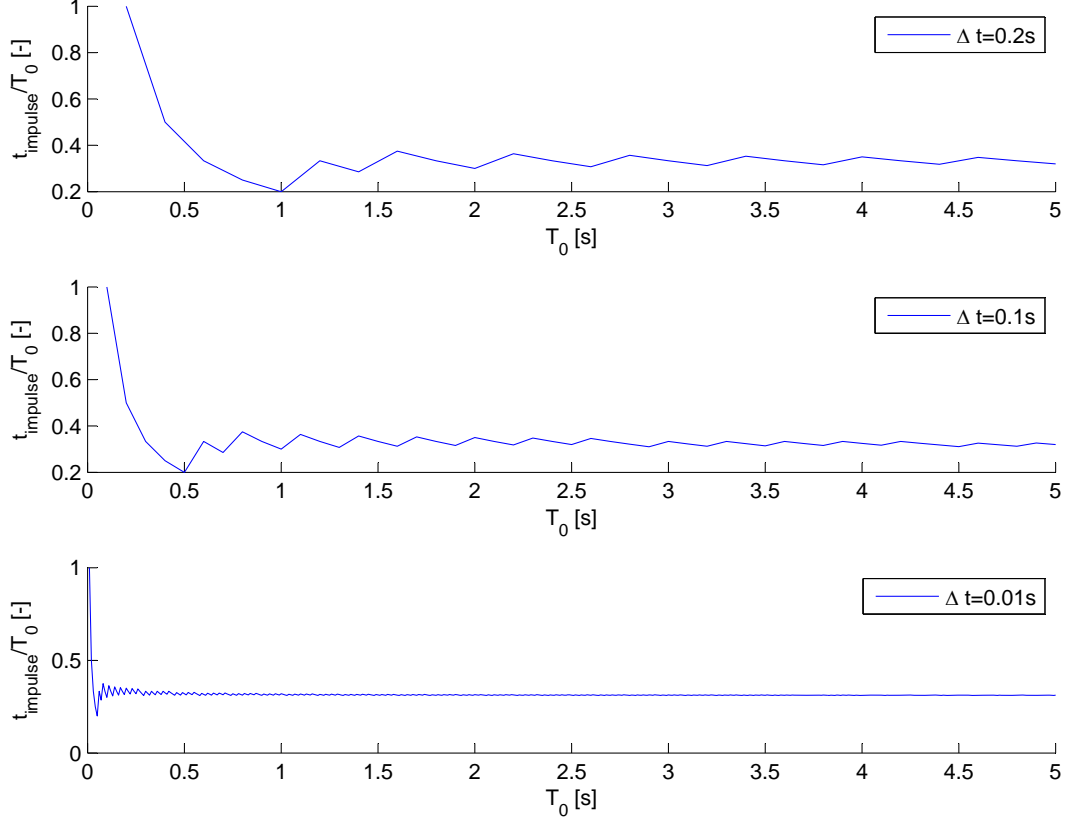


**Figure 2.9.** Ratio between impulse load duration  $t_{impulse}$  and natural period  $T_0$ , as function of natural periods. Each of the plots are with different step size  $\Delta t$ .

As seen in Figure 2.9, the variation in  $\frac{t_{impulse}}{T_0}$  seems to decrease as the natural period gets higher independent of the value of  $\Delta t$ .  $\Delta t$  is the incremental time step size used in the time integration. This is due to the fact that an incremental time step forms a smaller and smaller proportion of the load duration  $t_{impulse}$ , as the natural period of the system increases. I.e. the error is greater at the lower natural periods.

Secondly, it is seen that the same number of time steps is required to get a steady value of  $\frac{t_{impulse}}{T_0}$  independent of  $\Delta t$ . A lower time step size  $\Delta t$  gives a wider span of natural periods, where the ratio  $\frac{t_{impulse}}{T_0}$  is approximately constant. This however requires more calculations.

Furthermore it is seen, that  $\frac{t_{impulse}}{T_0}$  is equal to one, as  $T_0$  equals the time step  $\Delta t$ . This means, that the snap-through has happened within the first time step in the integration.

Thus, it is evident to conclude, that the ratio between  $t_{impulse}$  and  $T_0$  is constant for a given load ratio, provided that  $T_0$  is significantly larger than  $\Delta t$  ( $\frac{T_0}{\Delta t} > 50$ ). Variation is due to inaccuracy caused by the numerical integration method. I.e. the time, for which

an impulse load has to be applied to cause snap-through, is proportional to the amount of mass, that has to be moved and inversely proportional to the size of the applied load.

### 2.2.2 Ramped loading

The load is now linearly ramped over time  $t_{ramp}$ , and then instantaneously removed, as illustrated in Figure 2.6(b). This makes it possible to prevent large accelerations and velocities and thereby imitate the static load scenario, or at least get very close. The structural properties listed in Table 2.1 and 2.2 are used in this part of the analysis as well. The ratio between  $t_{ramp}$  and natural period  $T_0$  as function of load ratio is seen in Figure 2.10.

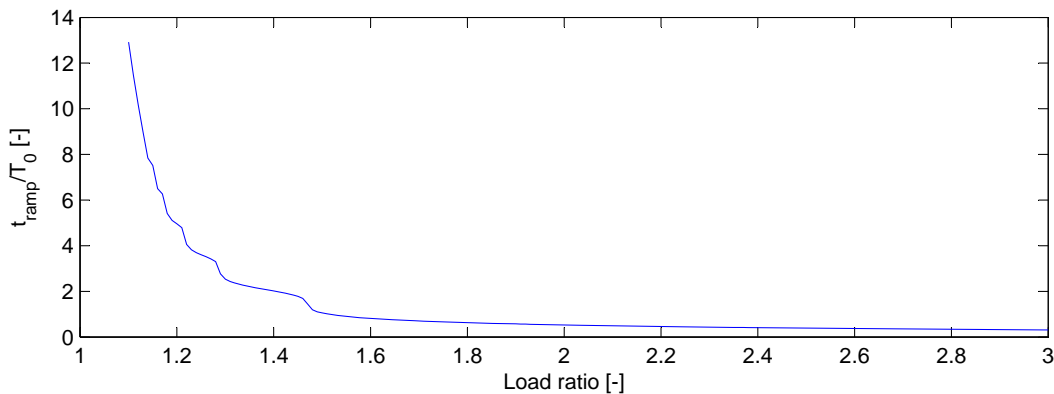


**Figure 2.10.** The ratio between  $t_{ramp}$  and natural period  $T_0$  as function of load ratio.

It is seen, that  $t_{ramp}$  approaches infinity, when the load ratio approaches one. This means, that the load is applied in such a slow manner, that the dynamics of the system becomes negligible. The uneven tendency in the graph at load ratios between approximately 1.15 and 1.5, can be explained by the interference between the natural harmonic motion of the structure and the load ramping. This interference can either amplify or reduce the motion corresponding to the steep and flat parts on the graph in the mentioned load ratio interval.

### 2.2.3 Harmonic loading

It is known that harmonic loading, with periods close to the natural periods of a structure, can have significantly larger effects in the structural behaviour compared to a static load with same magnitude. This is known as resonance. A sinusoidal load with amplitude varying from zero to a desired load ratio is applied, see Figure 2.6(c). Figure 2.11 shows the normalized maximum nodal displacement as function of the normalised load period with a load ratio equal to 0.1. As seen in the Figure, the load ratio 0.1 cannot cause snap-through. The maximum deformation is found within a time series of 400 seconds. This is done in order to ensure, that the displacement pattern is fully developed.

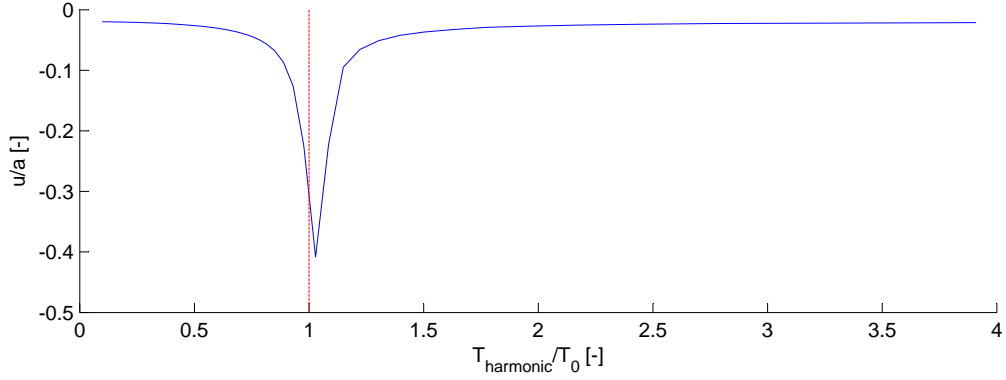


**Figure 2.11.** Structural response of structure with harmonic loading. The largest nodal displacement is normalized with the initial structural height  $a$ , and the load period is normalized with the natural period of the system. The load ratio is equal to 0.1. Snap-through does not happen.

It is apparent, that the biggest displacement is present, when the load period is slightly higher than the natural period. This is consistent with the fact, that the structural stiffness decreases as function of the downward nodal displacement ( $0 < u < -2$ ). The structural response to harmonic loading with  $T_{harmonic} = T_0$  over 400 seconds is seen in top of Figure 2.12. The asymmetry around the initial configuration ( $u=0$ ) is due to the nonlinearity of the system.

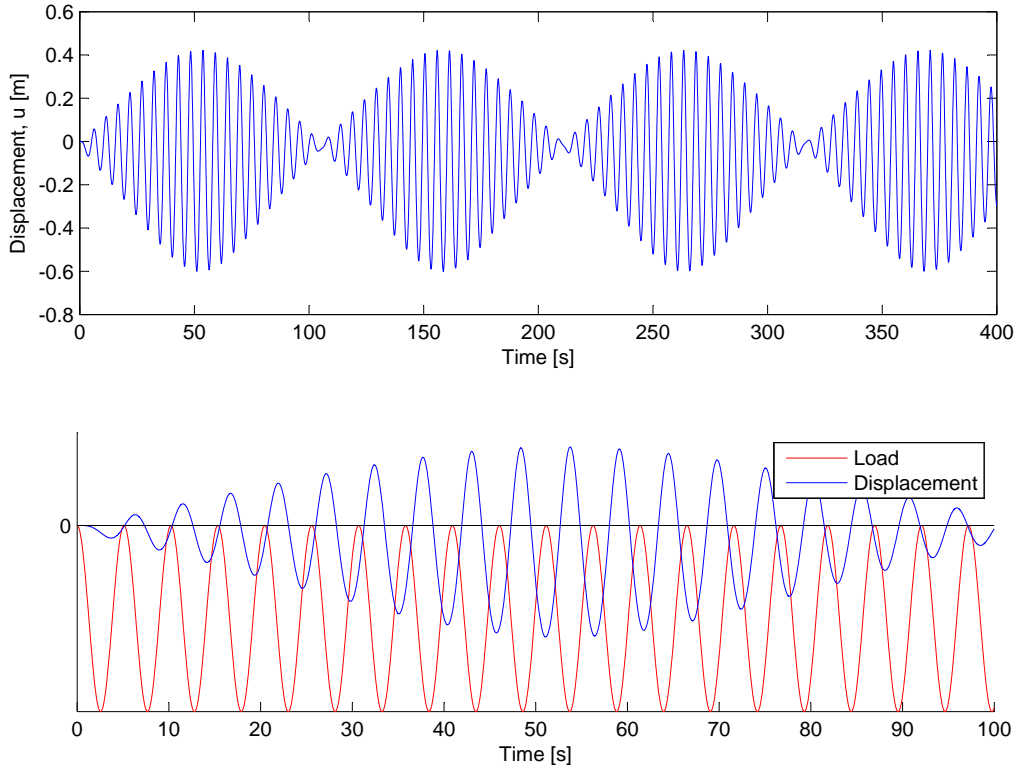


**Figure 2.12.** Structural response of structure with  $T_{harmonic} = T_0$ , and a load ratio of 0.1. The upper graph is nodal displacement over 400 seconds, while the lower graph displays the nodal displacement over 100 seconds. The lower graph is made in order to illustrate the influence of the load period on the structural behaviour.

The lower graph has the purpose of illustrating the relationship between the displacement and the harmonic load. Y-axis label is hence omitted. The load accelerates the system until approximately 50 seconds, after which the load decelerates the system. This tendency is due to phase lag induced by the changing structural stiffness and the inertia of the system in general. This pattern is repeated four times over the time span, 400 seconds. Harmonic loading with load ratios as low as 0.4 causes the structure to snap-through, see Figure 2.13.

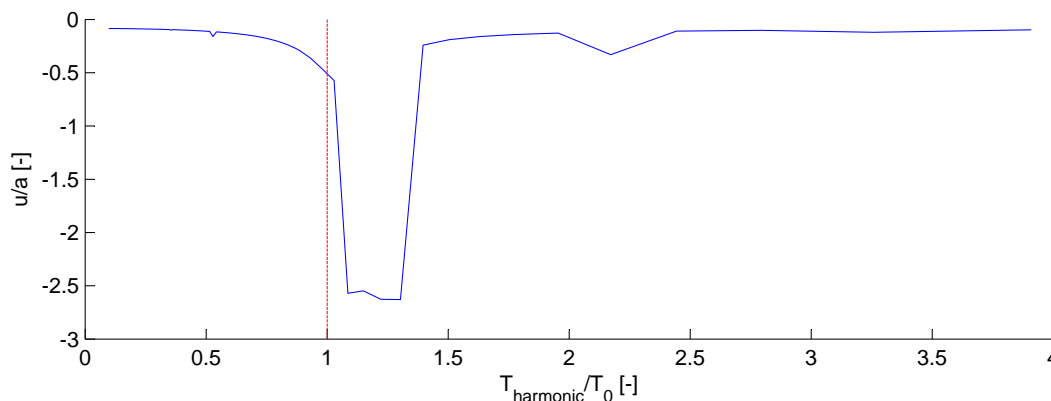


**Figure 2.13.** Structural response of structure with harmonic loading. The largest nodal displacement is normalized with the initial structural height  $a$ , and the load period is normalized with the natural period of the system. The load ratio is equal to 0.4.

It is again seen, that the biggest displacements are present, when the load periods are slightly bigger than the natural period. An even higher load ratio would provide a wider range of load periods, which would cause snap-through.

#### 2.2.4 Concluding remarks

Results have shown that the following parameters are affecting the structural behaviour:

- The time for which an uniform impulse load can be applied before limit load buckling, is proportional to the amount of mass that has to be moved and inversely proportional to the size of the load. As seen in Figure 2.8, it is possible to a load ratio below 1 (as low as 0.76) to cause snap-through.
- If the load is ramped over the time  $t_{ramp}$  until the load ratio is equal to one, the time required to cause snap-through equals infinity. I.e. the load is applied infinitely slow and the dynamics of the system vanishes.
- The structural response to a harmonic load is clearly affected by resonance. The nonlinearities of the structure cause phase lag between load and displacement. Calculations shows that a load ratio as low as 0.4 can cause snap-through.

This knowledge about the structural response to different load types will now be used as basis for for further finite element calculations on a wind turbine tower.

## CHAPTER 3

---

# Modelling of Wind Turbine Tower

---

The basis for dynamic buckling analysis of the wind turbine tower is presented in Chapter 2. It is observed, that the time, for which a load can be applied before limit load buckling, is proportional to the amount of mass that has to be moved and inversely proportional to the size of the load. This knowledge about the influence of certain parameters in the structural behaviour of the simple truss is now used in an analysis of a full-size finite element modelled wind turbine tower.

The structural behaviour of a tower is analysed with both simplified time-varying loads and more realistic simulated wind loads. Finite element analyses are carried out in the commercial finite element program, Abaqus. When developing the finite element formulation, the goal is to keep the computational cost and time on a minimum, while having an adequate level of accuracy in the numerical model. An introduction of unnecessary elements or degrees of freedom (DOF) should be avoided if the gained accuracy is negligible in relation to the problem and the desired result. This is the aim of a convergence analysis, which is performed in section 3.4.

This chapter presents the properties of the considered tower and the assumptions made. Used elements and considerations of model discretisation is presented in the chapter as well.

### 3.1 Tower properties and boundary conditions

Preliminary dimensions of a 3MW wind turbine tower is provided, and can be found in Appendix B.1. The tower has a conical shape and total height of 61.8m. The outer diameter of the tower is varying from 4.538m to 3.258m, and the wall thickness is varying from 0.014m to 0.05m. It is assumed, that the mass of the tower interior can be approximated by lumped masses illustrated with horizontal lines on the tower in Figure 3.1, and by adding 7.1% to the steel density. Magnitudes of lumped masses and the additional density is recommended by the turbine manufacturer, and are presented in Table 3.1. The weight of nacelle and rotor will be added as a lumped mass at the top of the tower with a total magnitude of  $350 \cdot 10^3$ kg. Inertia effects from nacelle and rotor

must be added to the model in order to justify this assumption. Inertia considerations are described and defined in section 3.2.

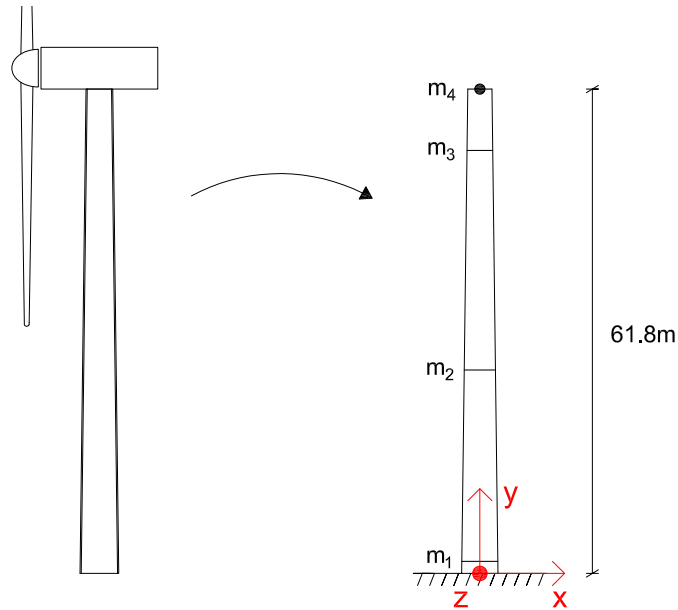


**Figure 3.1.** Sketch of the turbine tower simplification. Lumped masses  $m$  are distributed to nodes at horizontal lines illustrated in the Figure. The Figure is not correct scaled.

$m_1, 0.09\text{m}$	1925 kg
$m_2, 25.25\text{m}$	2076 kg
$m_3, 56.66\text{m}$	6000 kg
$m_4, 61.80\text{m}$	2005 kg
Nacelle mass	$240 \cdot 10^3$ kg
Rotor mass	$110 \cdot 10^3$ kg

**Table 3.1.** Lumped masses and their position on the y-axis.

Nodes at the top edge of the tower are tied to a reference point in order to maintain the relatively large stiffness at the point, where the nacelle is mounted. This causes no deformation of the top edge, but it still allows it to rotate and move as a rigid body with the tower. Lumped masses which represent nacelle and rotor are placed in the reference point as well. The tower bottom is modelled as fixed in all DOF. The reference point and the tied nodes are seen in Figure 3.2.

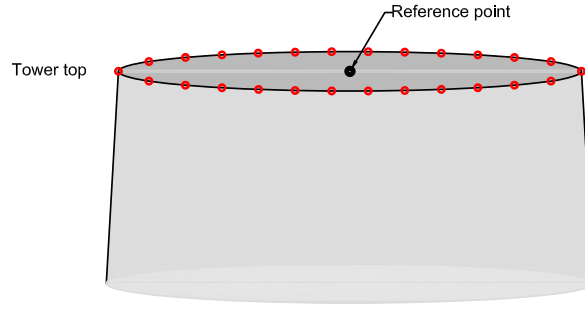


**Figure 3.2.** Tower top with reference point and tied element nodes.

Assumed material properties are presented in Table 3.2.

Steel density, $\rho$	7800 kg/m <sup>3</sup>
Model density	8354 kg/m <sup>3</sup>
Elastic modulus, E	200·10 <sup>9</sup> Pa
Poisson's ratio, $\nu$	0.3 [-]

**Table 3.2.** Material properties.

## 3.2 Inertia considerations

In order to make a realistic dynamic model of the wind turbine, it is important to include inertia effects of nacelle and rotor. The mass and second mass moments of inertia of the nacelle and rotor are applied in the reference point, as illustrated in Figure 3.2. It is important to notice, that this is a rough approximation of the real physical properties of the wind turbine, but it includes the large dimensions and masses of the nacelle and rotor. Properties from a similar 5MW wind turbine are used to estimate second mass moments of inertia around all three axes of the local coordinate system at the reference point  $(x_{RP}, y_{RP}, z_{RP})$ , see Figure 3.3. The 5MW wind turbine is a reference model used by the National Renewable Energy Laboratory (NREL) [Jonkman et al., 2009]. It is assumed, that properties of the 5MW wind turbine are suitable for the model even though the tower is from a 3MW wind turbine. This is done, since it is unclear, how the wind turbine capacity is related to the structural dimensions, especially between different manufactures.

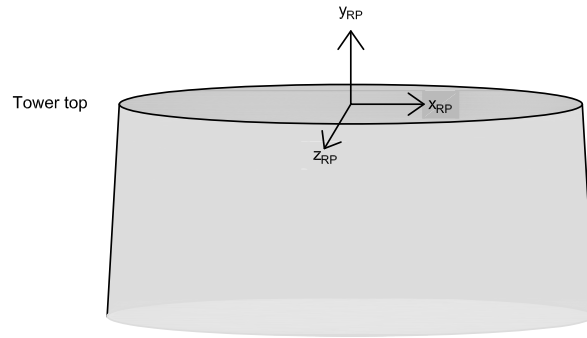


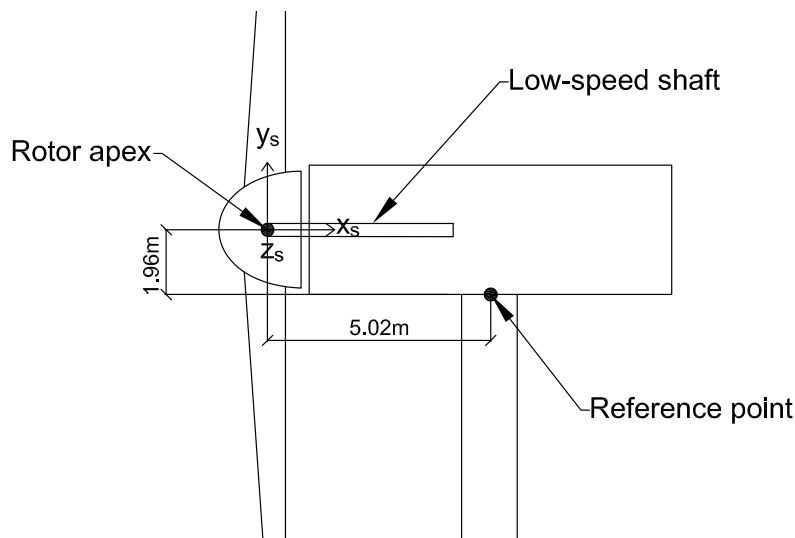
**Figure 3.3.** Local coordinate system at reference point.

Information of the second mass moment of inertias in the 5MW reference model is given in Table 3.3.

$I_{Nacelle}$ , Nacelle inertia about yaw axis (corresponds to $y_{RP}$ )	2,607,890 kg·m <sup>2</sup>
$I_{Blade}$ , Blade inertia about $x_s$	11,776,047 kg·m <sup>2</sup>
$I_{Hub}$ , Hub inertia about $x_s$	115,929 kg·m <sup>2</sup>

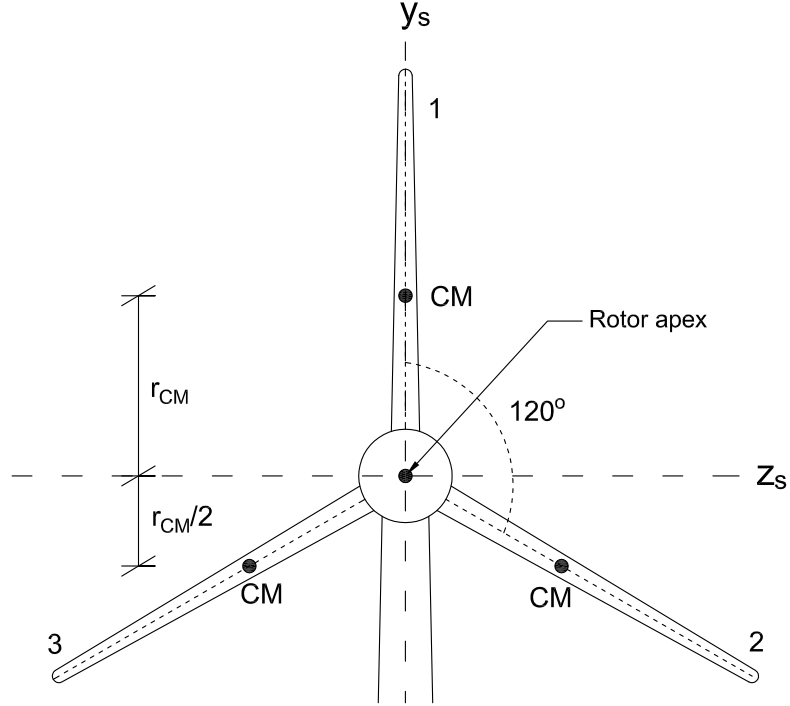
**Table 3.3.** Second mass moments of inertia from NREL 5MW reference wind turbine [Jonkman et al., 2009].

Figure 3.4 shows the location of the shaft coordinate system ( $x_s, y_s, z_s$ ).



**Figure 3.4.** Location of shaft coordinate system, with respect to the reference point.

Magnitudes of the second mass moments of inertia at the reference point are estimated from the values in Table 3.3. Inertia around the  $y_s$  and  $z_s$  axis is assumed to be one and a half times the inertia of a single blade, plus nacelle inertia around the yaw axis. The assumption of  $3/2$  of the blade inertia is based on geometrical considerations of the rotor, see Figure 3.5.



**Figure 3.5.** Geometrical definitions used for determination of inertias. CM is the center of mass of the blades.

The vertical distance  $r_{CM}$  from the  $z$ -axis to the center of mass of the three blades, is illustrated in Figure 3.5. Second mass moment of inertia is defined as mass times the squared distance to the considered axis. From Figure 3.5 it is seen that contributions to inertia about  $z_{RP}$  from blade 1, 2, and 3 would be 1, 0.25, and 0.25 respectively. Values from the reference model listed in Table 3.3 are second mass moments of inertia from hub and nacelle about the  $x_s$ -axis. These inertias are converted to inertias about the reference point using the parallel-axis theorem, which is the original inertia plus mass times the squared distance to a parallel axis. Inertia contributions from the conversion of shaft coordinate system to the reference point are given in Table 3.4.

$I_x, x_s$ to $x_{RP}$	$110 \cdot 10^3 \text{ kg} + (1.96\text{m})^2$	$422,576 \text{ kg} \cdot \text{m}^2$
$I_y, y_s$ to $y_{RP}$	$110 \cdot 10^3 \text{ kg} + (5.02\text{m})^2$	$2,772,044 \text{ kg} \cdot \text{m}^2$
$I_z, z_s$ to $z_{RP}$	$I_x + I_y$	$3,194,620 \text{ kg} \cdot \text{m}^2$

**Table 3.4.** Contributions from the Parallel-axis theorem.

Due to a lack of information about the inertia of the nacelle about the  $x_{RP}$ -axis, it is assumed, that this corresponds to  $1/4$  of  $I_{Nacelle}$ . An overview of the applied inertias is given in Table 3.5.

Inertia axis	Contributions	Value
$x_{RP}$	$3 I_{Blade} + 1/4 I_{Nacelle} + I_x$	$36,518,615 \text{ kg} \cdot \text{m}^2$
$y_{RP}$	$3/2 I_{Blade} + I_{Nacelle} + I_y$	$23,044,004 \text{ kg} \cdot \text{m}^2$
$z_{RP}$	$3/2 I_{Blade} + I_{Nacelle} + I_z$	$23,466,580 \text{ kg} \cdot \text{m}^2$

**Table 3.5.** Second mass moments of inertia at the reference point.

### 3.3 Finite element modelling

It is chosen to model the wind turbine tower with shell elements. This is assumed reasonable since two dimensions are significantly larger than the third. The use of solid elements to model a thin-walled structure would also require a finer mesh in order to avoid initial too distorted solids with an unacceptable aspect ratio. The use of solid elements would make it possible to analyse structural features in all directions, but would require an equivalent longer computational time.

A shell element is characterized by its ability to model in-plane and out-of-plane deformations, referred to as membrane and bending deformations. The two basic theories for shells are similar to the two plate theories formulated by *Kirchhoff* in 1850 and *Mindlin* in 1950, with the exception of the shells additional ability to model membrane deformations. A shell can be considered as a combination of a plate and a 2D plane-stress element.

The *Kirchhoff-Love* shell theory does not account for transverse shear deformations, while the *Mindlin* shell theory does. The two theories can be considered equivalents to the Bernoulli-Euler beam theory and the Timoshenko beam theory. The contribution to the deformation from transverse shear, increases with increasing element thickness and is negligible for very thin shells, which is why, the theories are referred to as thin-shell and thick-shell theories as well. Thickness is a relative measure and should be seen in relation to the span of the shell [Nielsen et al., 2007] [Cook et al., 2001].

The fundamental difference in the derivation of the two shell theories is the assumptions of cross sectional behaviour. The thin-shell Kirchhoff shell theory states, that a line which is initially straight and normal to the midsurface, remains straight and normal to the midsurface at a deformed state. The Mindlin plate theory however allows rotation of the cross section, which means, that a midsurface normal does not stay normal. I.e. differences between rotation of midsurface normal and slope of plate surface.

There is no specific limit that separates thin from thick shells, but it is recommended to use thick shell theory, when the ratio between the characteristic length and thickness of the shell is less than 15 [Simulia, 2011]. It is chosen to use thick-shell elements in order to capture all features of the elements, including deformations from transverse shear. It is chosen to use quadratic 8-noded shell elements to model the tower, since their second order shape functions behaves well under bending deformation. The element is shown in Figure 3.6.

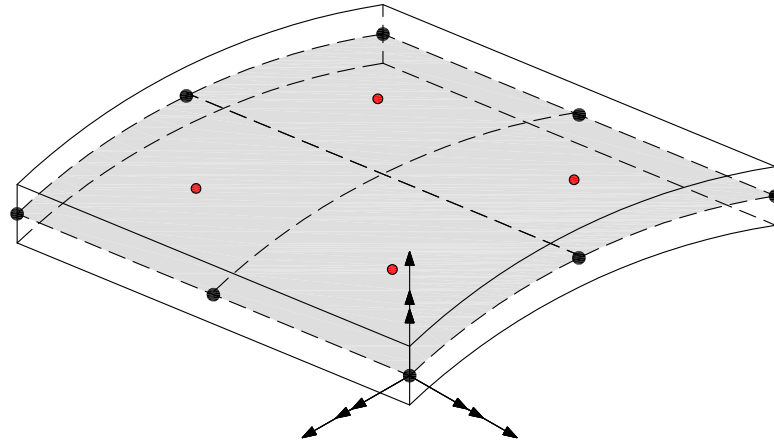


**Figure 3.6.** Quadratic 8-noded shell element. Nodes and integration points are illustrated with black and red dots respectively. The grey area is the midsurface of the element. Three rotational and three translational DOF are illustrated in one of the nodes. The elements has 48 DOF in total.

It is though unclear, how fast linear elements will converge compared to quadratic elements. Beside the ability to model bending deformation, the 8-noded quadratic element does not suffer from spurious modes and locking. An under-integrated linear element suffers from a spurious mode called hourglassing, where the strain energy in the single integration point is zero, which would give poor results. Fully integrated linear elements, which are subject to bending, suffer from shear-locking, where the element behaves too stiff.

The wind turbine tower deforms with relative large deformations and the assumption of infinitesimal strains is not adequate. The structural stiffness is no longer constant and the displacement-dependent stiffness matrix must be updated in each load step. When solving a geometrical nonlinear problem iteration has to be used. There are different iteration schemes available, but it is chosen use the "Arc-length method". This method is used, since it can capture post-buckling behaviour of the structure. It is verified, that the pre-buckling behaviour and buckling value is identical, when the analysis is carried out with different iteration schemes. A brief description of different iteration schemes can be found in Appendix C.

It is obvious, that the simple truss and the full size modelled finite element tower are complete different in dimension (2D and 3D), geometry, size, and complexity. In spite of that, it is assumed, that the two structures are comparable and will exhibit a common limit load buckling response pattern. When the horizontal load has reached the limit buckling load, a further increase in load will results in a similar snap-through motion with corresponding large deformations.

### 3.4 Convergence analysis

A convergence analysis is performed in order to ensure, that the output of the finite element analysis approaches a single solution, as the mesh is refined. A satisfactory mesh, is a mesh that provides a result, which is no or negligible different than a result obtained with an even finer mesh. The analysis is carried out by increasing the number of 8-noded quadratic elements in the model and finding the buckling load to each mesh. The load is applied as a static horizontal load acting parallel to the x-axis at the reference point. The reference point distributes the load to nodes at the edges of the top shell elements, as seen in Figure 3.2. The buckling load is found by a geometrical nonlinear analysis. It is assumed, that the buckling has occurred, when the load-displacement curve reaches a maximum, i.e. tangent stiffness matrix becomes singular. Displacement is in terms of horizontal displacement of reference point.

The aspect ratio, which is the ratio between the height and length of elements, is limited to 1:2, since it is important to avoid initially distorted elements. Initially flat, skew or strongly curved-sided elements will tend to decrease accuracy of the results. Abrupt changes in neighbouring elements sizes should be avoided as well [Cook et al., 2001]. Results are presented in Figure 3.7

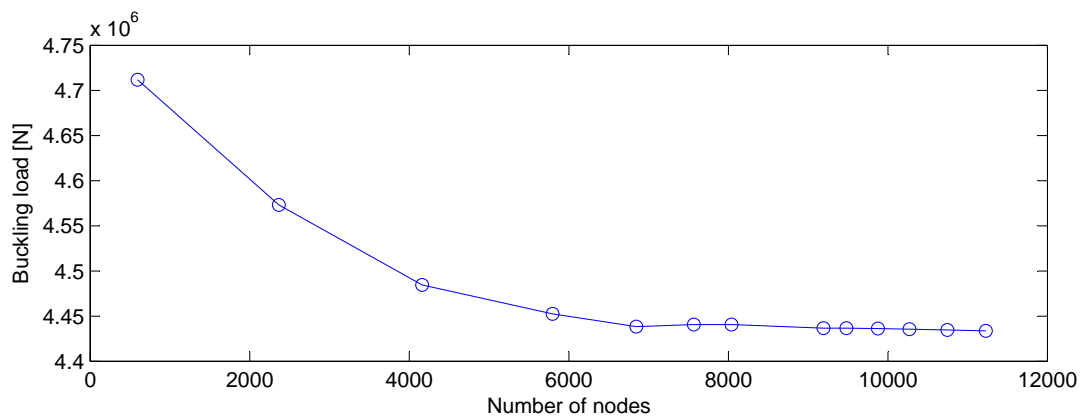


*Figure 3.7.* Convergence analysis of mesh refinement.

It is assumed that the satisfactory solution is achieved with 6846 nodes, corresponding to 2268 elements. This mesh is seen in Figure 3.8. A mesh refinement from 6000 to 11000 nodes will only change the results with about a half percent. The static buckling load is found to  $4.4338 \cdot 10^3 \text{ kN}$ , and from an eigenvalue analysis the natural frequency and period of the wind turbine towers first fore-aft mode is found to  $f_0 = 0.25 \text{ Hz}$  and  $T_0 = 4.0 \text{ s}$ . The first fore-aft mode is seen in Figure 4.21.

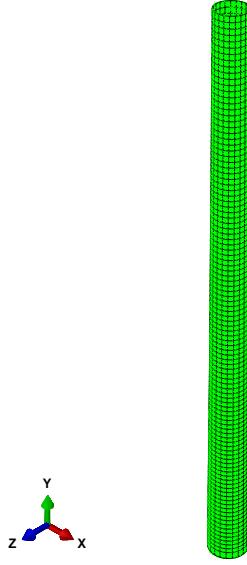


**Figure 3.8.** Mesh of tower model with 6846 nodes and 2268 quadratic 8-noded shell elements.

The nonlinear load-displacement relation of the reference point is shown in Figure 3.9. The relation is plotted until buckling occurs at  $P_{static} = 4.4338 \cdot 10^3 \text{kN}$ , and displacement  $u_x = 3.082 \text{m}$ .

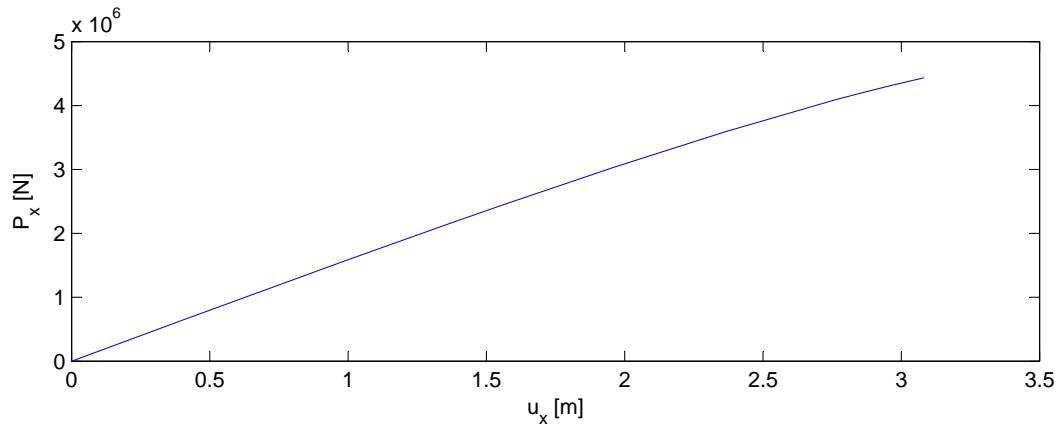


**Figure 3.9.** The load-displacement relation of tower at reference point found with static analysis.

The structure is modelled with an assumption of a perfect elastic material behaviour with no yielding point. This is done in order to maintain focus on geometrical nonlinearities and to keep the influence of other parameters on a minimum. Yielding of material would be an additional factor, which would affect the structural response. The maximum stresses in the tower in a pre-buckling state are about 850MPa, which exceeds the yielding point of the most common construction steel and even high quality steel. This means, that local yielding will happen before buckling, and instability would probably not determine the structural design. It is assumed that the following results and findings are valid, even though yielding would be present before buckling with a more realistic material model.



## CHAPTER 4

---

# Analysis with Simple Time-varying Loads

---

The influence of different parameters on the structural response of a simple truss was examined in Chapter 2. It was found, that the variation and duration of time-varying loads are important parameters to the structural response. Similar time-varying loads are applied to the tower in this chapter, see Figure 4.1.

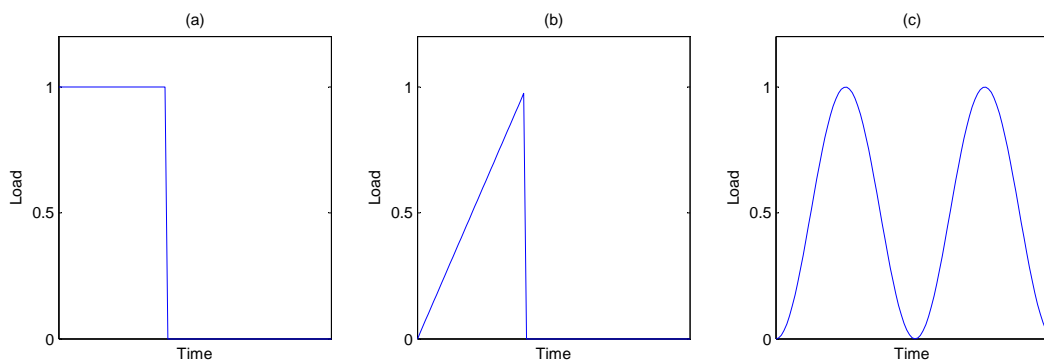


*Figure 4.1.* The three different time-varying load types: a) impulse, b) ramped, c) harmonic.

Loads do not propagate instantaneously in a dynamic analysis, and the development of deformations/stresses in the tower is a time dependent process. This is illustrated with an example in Figure 4.2 to 4.7. The Figures show the development of von Mises stresses in the tower as function of time. A horizontal time-varying point load of arbitrary magnitude is applied, and the tower does not buckle in this example.

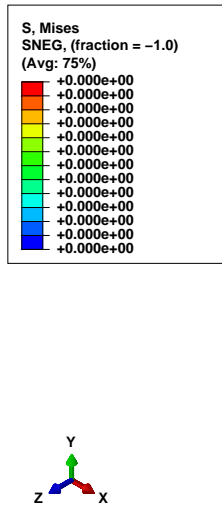


Figure 4.2. t=0s.

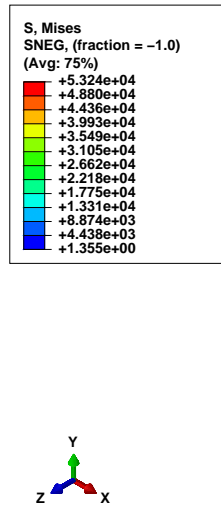


Figure 4.3. t=0.0012s.

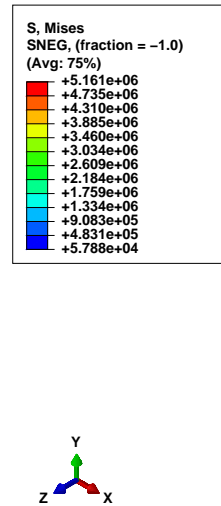


Figure 4.4. t=0.0529s.

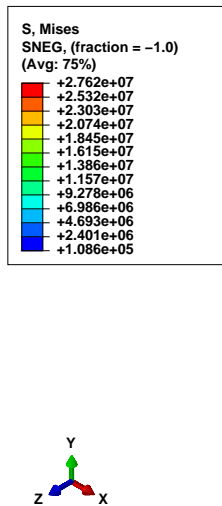


Figure 4.5. t=0.1891s.

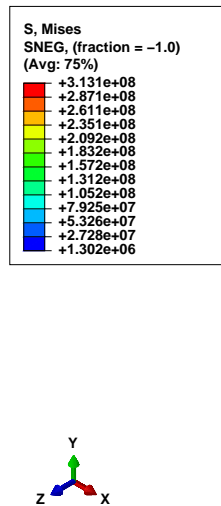


Figure 4.6. t=0.7291s.

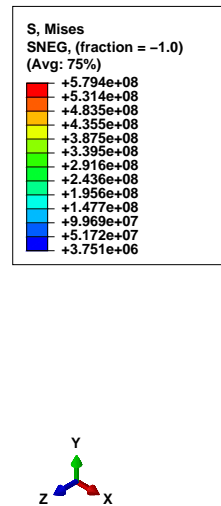


Figure 4.7. t=1.209s.

Dynamic analyses are performed using direct time integration to solve equation of motion (EOM), which is formulated as:

$$[M] \{\ddot{U}\} + [C] \{\dot{U}\} + [K] \{U\} = \{F_{ext}\} \tag{4.1}$$

where

$[K]$	Stiffness matrix
$[C]$	Damping matrix
$[M]$	Mass matrix
$\{U\}$	Displacement vector
$\{\dot{U}\}$	Velocity vector
$\{\ddot{U}\}$	Acceleration vector
$\{F_{ext}\}$	External force vector

Damping forces are not included in analysis of the three simple loads, but are included in Section 4.4. Time integration calculates the response at the next time step from EOM. There are two classifications of the integration algorithms, which can be used to solve EOM, namely explicit or implicit. Explicit algorithms use only historical information to solve the equation, and needs a sufficiently small time increment to be stable. Implicit algorithms are often unconditionally stable, and differ from explicit by the need of information of the next time step to calculate EOM at the current time step. A generalisation of an implicit Newmark algorithm is used. [Simulia, 2011] [Cook et al., 2001]

Analyses of the structural behaviour with the three time-varying loads are performed with the assumption of total energy conservation. An additional section with the inclusion of a damping model is presented, since it is unclear how damping affects the response. Furthermore it is analysed how imperfections will affect the structural behaviour by performing a imperfection sensitivity analysis with the presence of both static and time-varying loads.

## 4.1 Impulse loading

The load is applied as a horizontal impulse load (x-direction) with load duration  $t_{impulse}$ , and the minimum load duration which leads to buckling with a given load ratio is found. The time varying impulse load is seen in Figure 4.1(a), and Figure 4.8 shows the tower a moment after buckling has occurred.

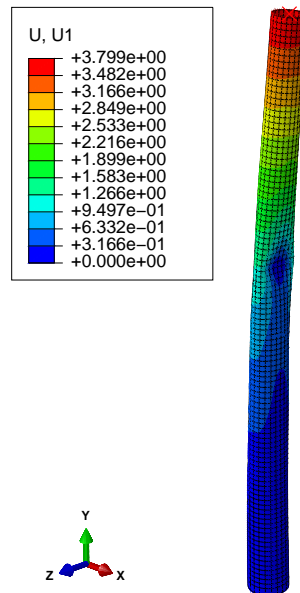


**Figure 4.8.** Deformed tower after buckling. The legend shows the displacement in the x-direction in meters.

It is not possible to identify the buckling load in the same manner as in the static case. The point (or time) of buckling is instead observed if or when the vertical (y-direction)

acceleration or velocity of the reference point, exhibits an abrupt change in magnitude over a relatively short period of time. This is illustrated in Figure 4.9.

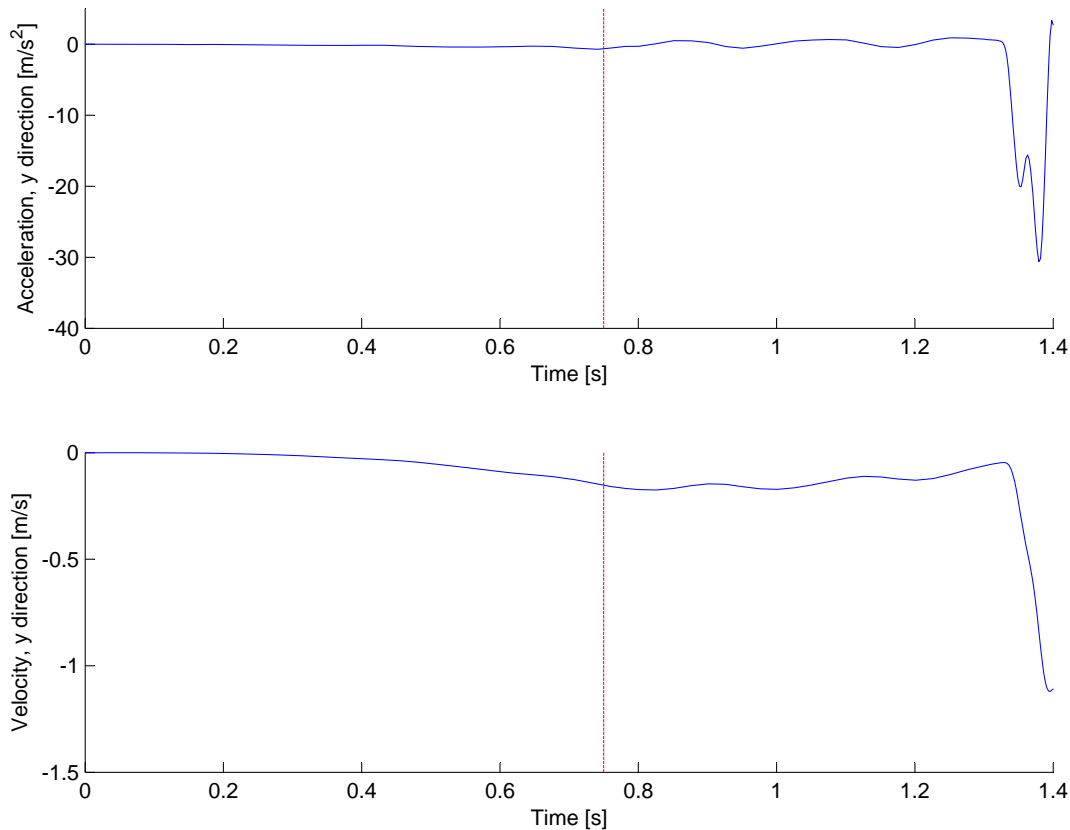


**Figure 4.9.** Vertical acceleration and velocity of reference point as function of time with a load ratio of 1. The load duration  $t_{impulse}$  in this example is 0.75 seconds (red line).

The ratio between load duration and natural period  $t_{impulse}/T_0$ , as function of load ratio is seen in Figure 4.10. The load ratio is again defined as the applied load divided by the static buckling load ( $4.4338 \cdot 10^3 \text{kN}$ ). It is evident, that the graph is similar to the graph in Figure 2.8.  $t_{impulse}$  decreases as the load ratio increases, and it is still possible to obtain buckling with load ratios below one.

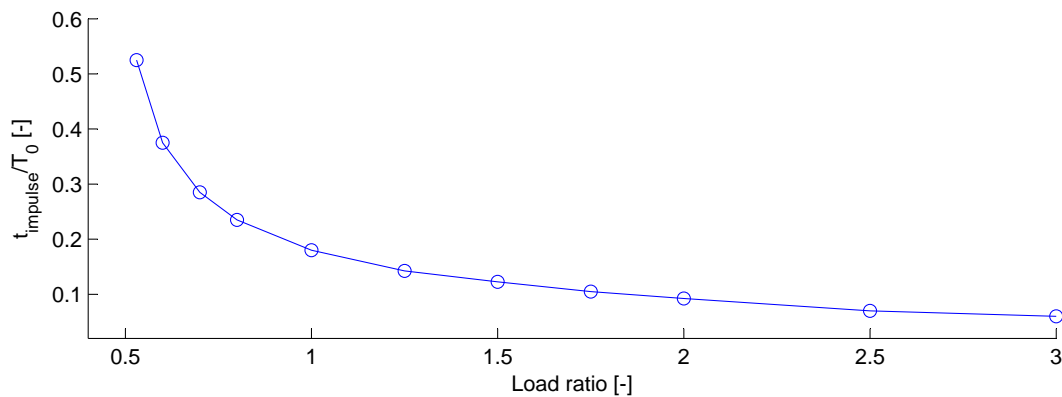


**Figure 4.10.** Ratio between impulse load duration  $t_{impulse}$  and natural period  $T_0$ , as a function of load ratios.

A load ratio of 0.53 is the lowest possible load, which causes buckling of the tower. The relation between load ratio and load duration indicates, that there is a certain amount of external energy required in cause buckling.

It is found, that load applied as an impulse load can have the same impact on the structure as a static load with almost twice the magnitude. This dynamic amplification is due to kinetic energy the system possesses during the induced motion. In order to avoid buckling, there must be enough potential strain energy in the whole system to decelerate the motion of the structure in a pre-buckling configuration. This level is defined as the maximum possible amount of strain energy, which can be stored in the tower without buckling. The maximum strain energy level  $E_{max}$  is found by static analysis to  $7.26 \cdot 10^6$ J, see Figure 4.11.

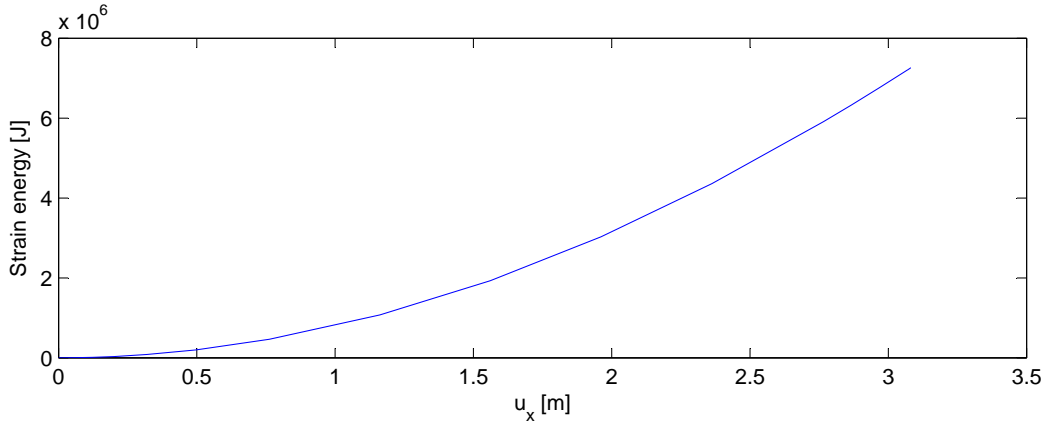


**Figure 4.11.** Strain energy development in tower found with static analysis. The highest level of strain energy defines  $E_{max}$ .

The energy developments of a buckled tower with a load ratio of 1 and a  $t_{impulse} = 0.75s$  is shown in Figure 4.12. External energy, strain energy, kinetic energy, and maximum strain energy are denoted  $E_{ext}$ ,  $E_{strain}$ ,  $E_{kin}$  and  $E_{max}$  respectively. It is seen, that the strain energy exceeds  $E_{max}$ , which is only possible in a buckled configuration.

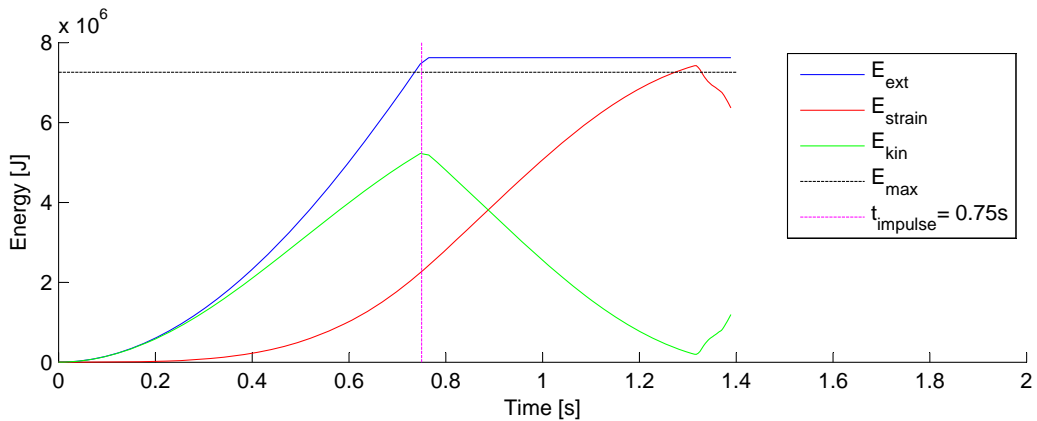


**Figure 4.12.** Energy developments of a buckled tower with a load ratio of 1. The post-buckling strain development is omitted in the graph.

If the load is removed a bit earlier ( $t_{impulse} = 0.73s$ , no buckling occurs and the strain

and kinetic energy of the system will outbalance each other as the tower sways back and forth, which is illustrated in Figure 4.13. This is of course based on the assumption of total energy conservation (no damping).

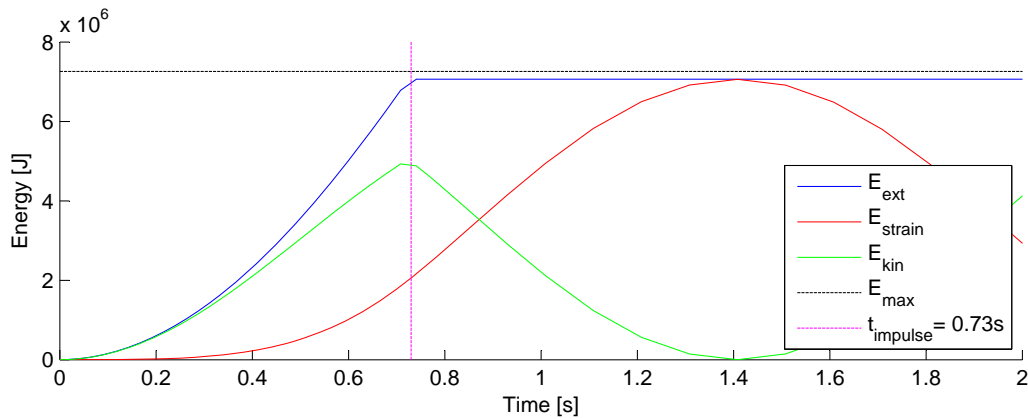


**Figure 4.13.** Energy developments of a non-buckled tower with a load ratio of 1.

Figure 4.10 shows the existence of a lower load ratio limit of 0.53. This load has to be applied for 2.1s, which is approximately half the natural period of the tower. If the load is applied more than half of the natural period, it decelerates the motion of the structure instead of accelerating. The load counteracts the motion and removes energy from the system. This is illustrated in Figure 4.14, where a load ratio of 0.5 is applied for 5s. The natural period  $T_0$  of the tower is 4s.

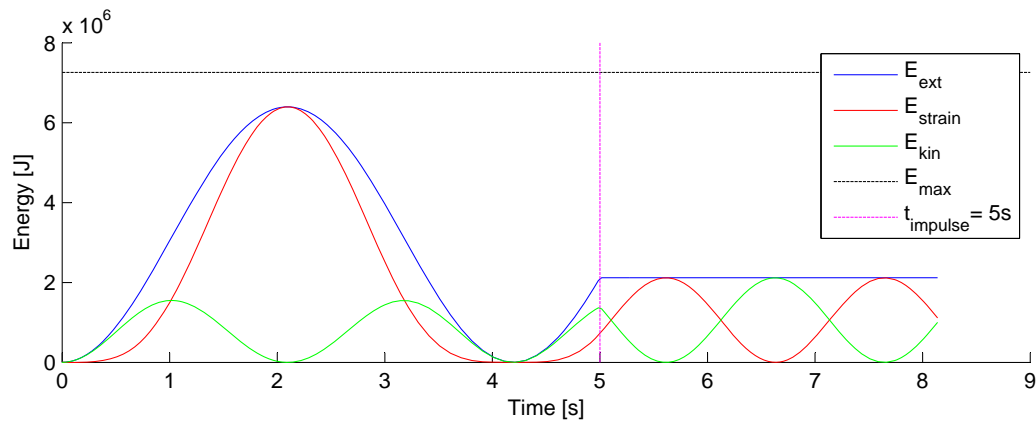


**Figure 4.14.** Energy developments of non-buckled tower with a load ratio of 0.5.

From these energy considerations it is evident that the buckling occurs, when all potential strain energy in the system has been utilised. This amount is constant for a horizontal point in the reference point, and is independent of whether energy comes from a large load with short duration or less load with long duration.

## 4.2 Ramped loading

The load is now linearly ramped over time  $t_{ramp}$  and then instantaneously removed, as illustrated in Figure 4.1(b). It is apparent, that buckling occurs if  $t_{ramp}$  coincide with the natural period of the tower. This amplification of the response is the reason for the uneven development of the graph in Figure 2.10, where the steep parts on the graph are caused by loading durations, which are in favour of the natural motion of the structure, when the load is removed. The flat parts on the curve in Figure 2.10 is where the load counteracts the motion of the structure the moment it is removed.

The response of the tower with a ramped load does not totally agree with the findings with the simple truss. It is possible for the tower to buckle with a load ratio below one (0.89), which is illustrated in Figure 4.15.

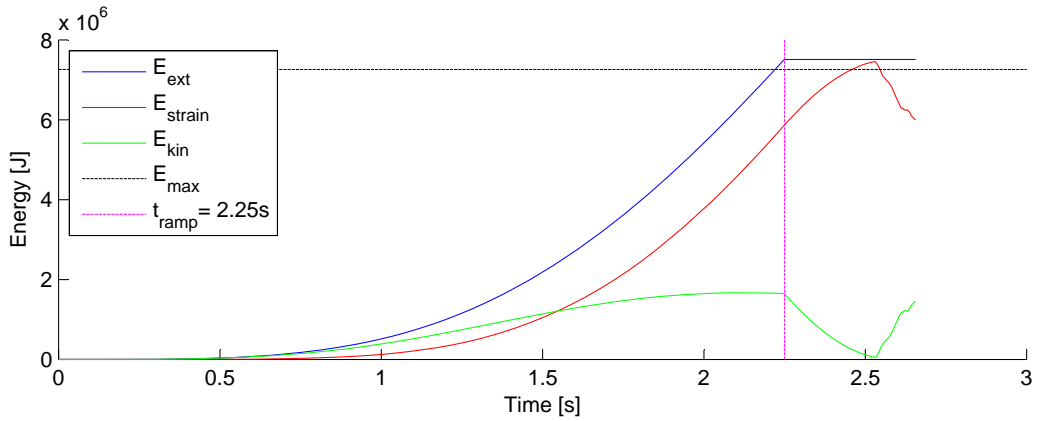


**Figure 4.15.** Energy developments of buckled tower with a load ratio of 0.89 and  $t_{ramp}=2.25s$ .

Buckling does not occur if the same load ratio is applied with  $t_{ramp}=T_0=4s$ , see Figure 4.16. This is due the fact that the load counteracts the natural motion of the tower, and that a ramped load in general induce less kinetic energy.

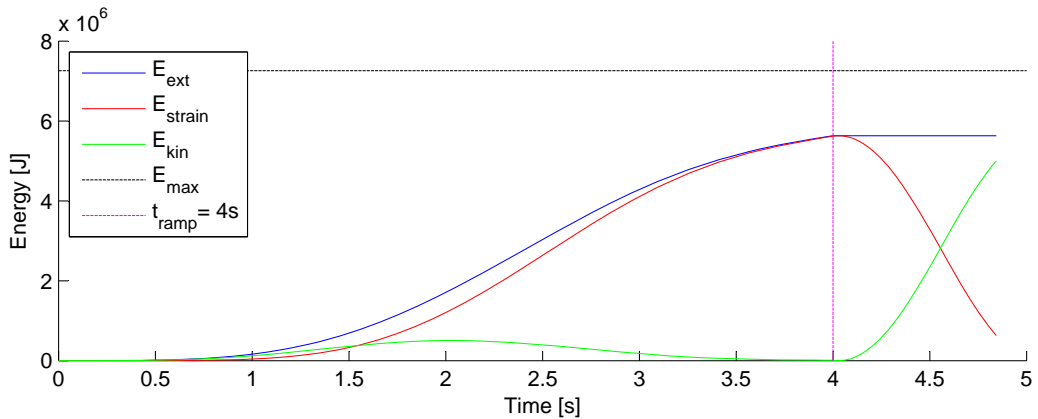


**Figure 4.16.** Energy developments of non-buckled tower with a load ratio of 0.89 and  $t_{ramp}=T_0=4s$ .

The load duration is now changed, so that the load is in favour of the natural motion, when

it is removed, such that  $t_{ramp}=T_0/2+T_0=6.25s$ . Buckling does not occur, even though the load is removed, when the kinetic energy is at a maximum. This is illustrated in Figure 4.17.

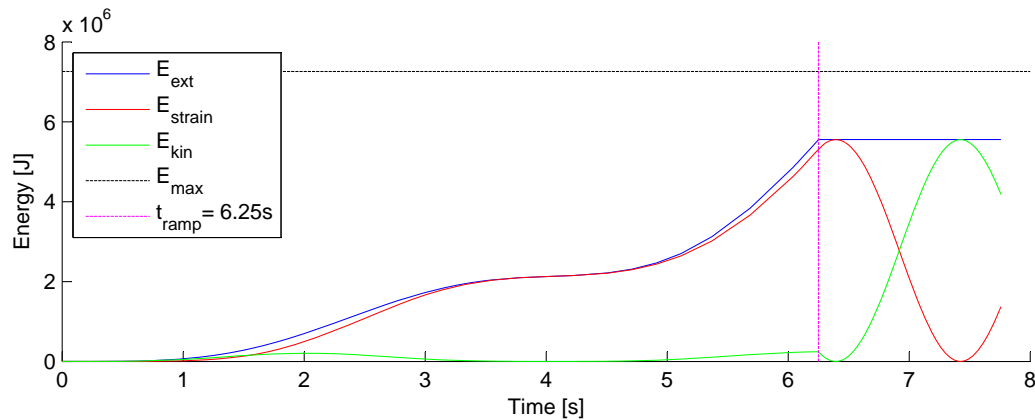


**Figure 4.17.** Energy developments of non-buckled tower with a load ratio of 0.89 and  $t_{ramp}=6.25s$ .

The results in Figure 4.15-4.17 shows, that a ramped load will have the greatest impact on the tower, when it is applied with a duration about half the natural period. This was also valid with a impulse load, but a  $t_{ramp} > T_0/2$  does not necessarily cause bigger displacements. If a ramped load is applied over long time, it will not induce any significant kinetic energy in the system, and will tend to act like a static load.

### 4.3 Harmonic loading

The load is again applied at the reference point but now as a harmonic load with characteristics seen in Figure 4.1(c). It is found, that a harmonic load with a load ratio as low as 0.1 can cause buckling if the period equals the natural period of the tower, and if the load cycle is repeated enough times. Energy is accumulated in the system each load cycle, and will eventually lead to buckling. The number of load cycles required for a given load ratio to cause buckling is plotted in Figure 4.18.

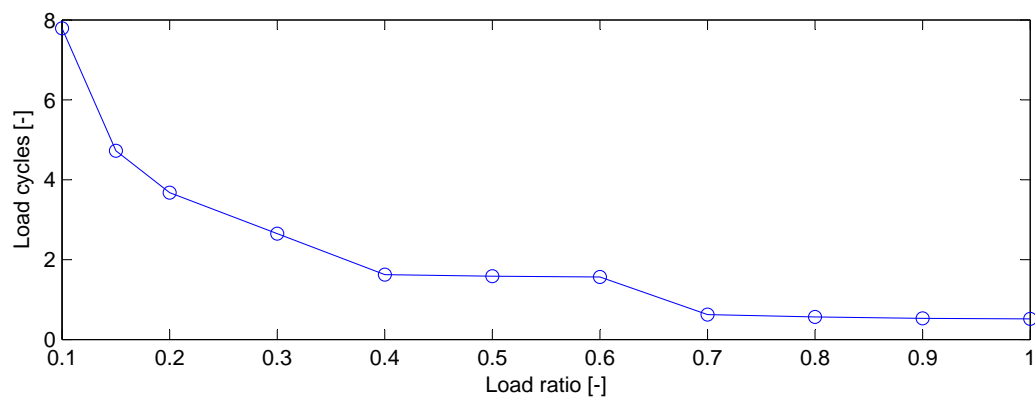


**Figure 4.18.** Number of load cycles needed to cause buckling.  $T_{harmonic} = T_0 = 4s$ .

An example is illustrated in Figure 4.19, where a load ratio equal to 0.2 causes buckling after approximately 15 seconds (3.75 load cycles).

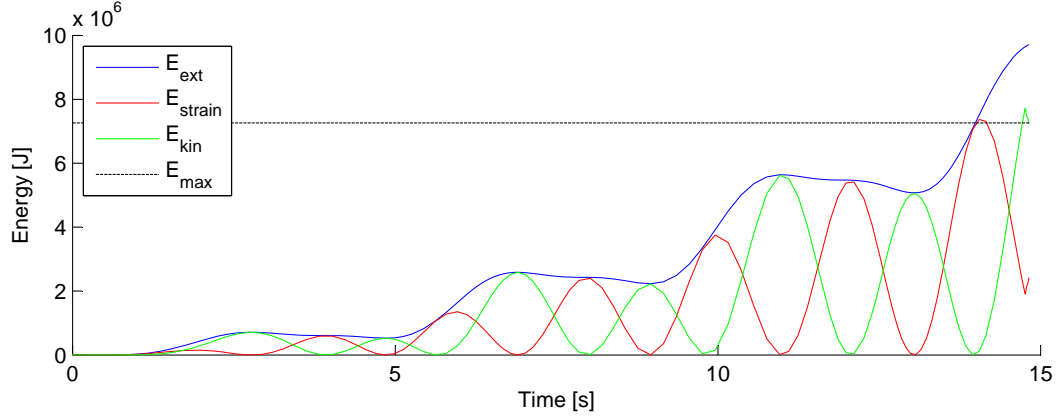


**Figure 4.19.** Energy developments in the system with harmonic loading. Load ratio equals 0.2. 3.75 load cycles are needed to cause buckling.

In examination of the simple truss (Figure 2.12) it was found, that there is a lower limit of load ratio (0.4), which causes buckling. It is not possible to find a similar limit for the tower. This is due to the fact that stiffness of the tower in the pre-buckling configuration does not change as significantly as in the simple truss. The degree of nonlinearity in the simple truss is greater than in the tower.

The load will add energy to the system in each cycle, and even very small loads can cause buckling, given that the number of load cycles is corresponding large. This is again based on the assumption of total energy conservation.

## 4.4 Damping of structural response

Previous results are all obtained without taking energy dissipation in the system into account. This section examines the response of the tower with an inclusion of a linear viscous damping model, which assumes, that energy dissipation is proportional to velocities as seen in Equation 4.1. The analysis is carried out with the application of a horizontal impulse load as in Section 4.1.

The used damping model assumes, that the damping matrix,  $[C]$ , is proportional to the mass and stiffness of the structure. This type of damping is often referred to as Rayleigh damping:

$$[C] = \alpha [M] + \beta [K] \quad (4.2)$$

[Cook et al., 2001]

Damping coefficients  $\alpha$  and  $\beta$  are related to the damping ratios  $\xi_1$ ,  $\xi_2$  and the natural frequencies of the tower:

$$\alpha = 2\omega_1\omega_2(\xi_1\omega_2 - \xi_2\omega_1)/(\omega_2^2 - \omega_1^2) \quad (4.3)$$

$$\beta = 2(\xi_2\omega_2 - \xi_1\omega_1)/(\omega_2^2 - \omega_1^2) \quad (4.4)$$

The stiffness proportional part  $\beta [\mathbf{K}]$  of  $[\mathbf{C}]$  damps the highest frequencies the most, while the mass proportional part  $\alpha [\mathbf{M}]$  dominates with most energy dissipation from the lower frequencies [Alipour and Zareian, 2008]. This relation is illustrated in Figure 4.20, where the combined damping ratio is given by:

$$\xi = \frac{\alpha}{2 \cdot \omega} + \frac{\beta \cdot \omega}{2} \quad (4.5)$$

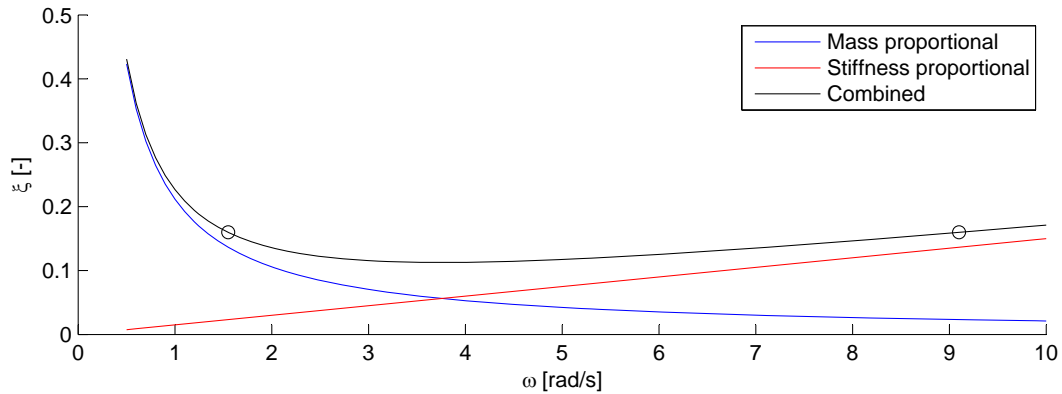


**Figure 4.20.** Relation between natural frequencies and damping ratio. The black circles indicate the range of interest. [Cook et al., 2001]

The natural frequencies of interest is chosen to be frequencies corresponding to second and fifth natural mode  $\omega_1=1.55\text{rad/s}$  and  $\omega_2=9.10\text{rad/s}$ . These frequencies corresponds to first and second "fore-aft" modes, which are modes, that are likely to be excited by the forces applied reference point. The two fore-aft modes are seen in Figure 4.21 and 4.22.

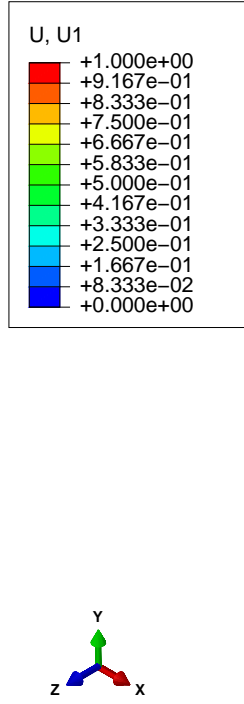


**Figure 4.21.** Second natural period of the tower denoted the 1st fore-aft mode,  $\omega_1=1.55\text{rad/s}$ .

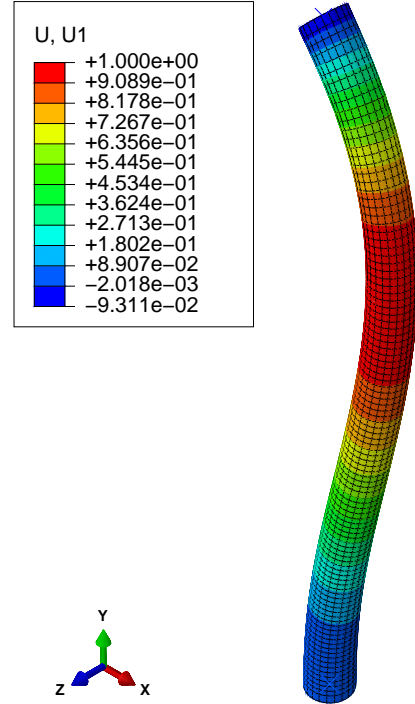


**Figure 4.22.** Fifth natural period of the tower denoted the 2nd fore-aft mode,  $\omega_2=9.10\text{rad/s}$ .

In most civil engineering structures damping ratios are typically between 0.02 and 0.1, and it is therefore chosen to use damping ratios in this order of magnitude [Williams and Todd, 2000]. Damping ratios  $\xi_1$ ,  $\xi_2$  are chosen to be of equal size, which implies the same damping of  $\omega_1$  and  $\omega_2$ . Values of  $\alpha$  and  $\beta$  found with different damping ratios are seen in table 4.1.

$\xi_1, \xi_2$ [-]	$\alpha$ [1/s]	$\beta$ [s]
0.01	0.0265	0.0019
0.02	0.0529	0.0038
0.04	0.1058	0.0075
0.08	0.2116	0.0150
0.16	0.4233	0.030
0.32	0.8465	0.060

**Table 4.1.** Damping coefficients found with  $\xi_1=\xi_2$ , and  $\omega_1=1.55\text{rad/s}$ ,  $\omega_2=9.10\text{rad/s}$ .

An example of the ratio between load duration and natural period  $t_{impulse}/T_0$  as function of load ratio is seen in Figure 4.23. The lowest load ratio, which causes buckling in the damped structure, is 0.59 (0.53 in the undamped case).

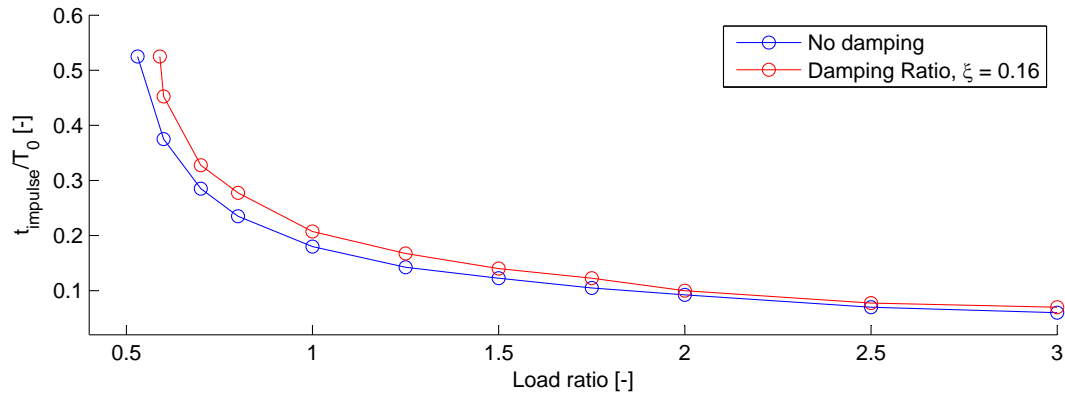


**Figure 4.23.** Ratio between impulse load duration  $t_{impulse}$  and natural period  $T_0$  as a function of load ratios in a damped and undamped case.

From the graphs in Figure 4.23, it is evident that the damped relation is similar to the undamped. It is found, that the maximum potential strain energy in the system increases, as the level of damping increases. Strain energy level as function of  $\xi$  is seen in Figure 4.24.

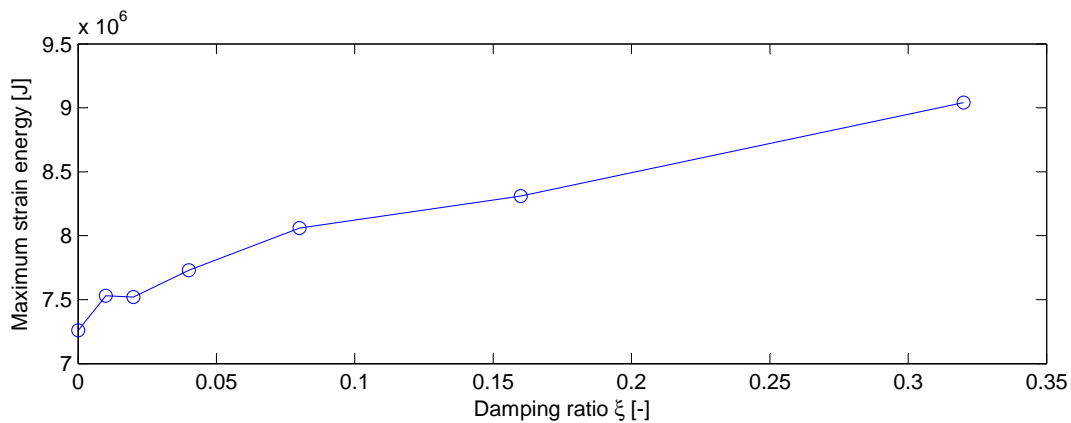


**Figure 4.24.** Maximum potential strain energy as function of damping ratio  $\xi$ .

The damping dependent energy level is caused by rearranged deformations in the structure introduced by the mass and stiffness proportional damping model. Figure 4.25 shows normalized horizontal deformations (x-direction) at various places at the tower measured from tower bottom. Deformations are normalized with respect to the undamped displacements, with a top (reference point) displacement of 3m in all cases.

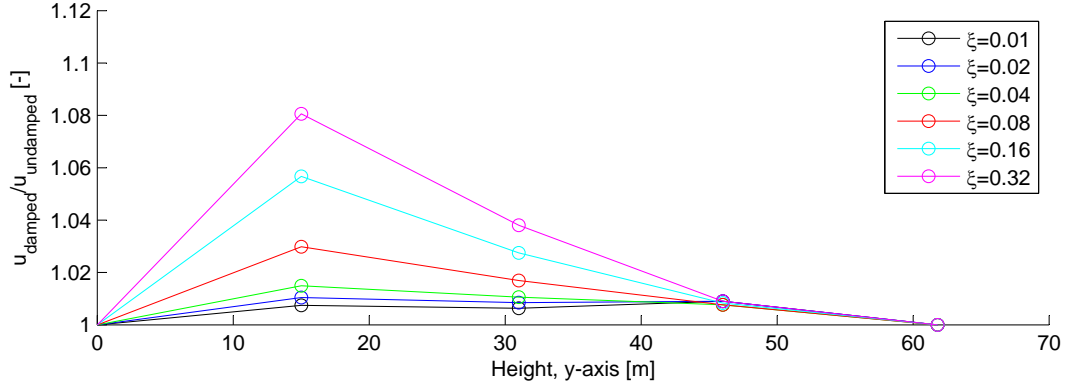


**Figure 4.25.** Normalized horizontal deformations, as function of tower height (y-direction) measured from the bottom.

The graphs illustrate that horizontal displacement in the middle of the tower increases with increasing damping ratio. From these findings it is apparent, that the response of an undamped structure is similar to the response of a damped structure. There is however differences in the displacement patterns, when damping is introduced, and the maximum strain energy increases with damping ratio.

## 4.5 Imperfection sensitivity analysis

As mentioned in Chapter 1 imperfections in structures are unavoidable, which is why, initial imperfection is an important parameter to consider in the modelling. It is though unclear how imperfection will affect a dynamic analysis compared to a static, and whether the structural response is any different with the introduction of imperfections.

Imperfections may arise during manufacturing process and could for example include welding seam, dents, variation in shell thicknesses, inhomogeneous material properties, residual stresses etc. The random nature of imperfections makes them difficult to predict, and structural design with such in consideration will always be based on assumed shapes, positions, and amplitudes of the imperfections. A method to include geometrical imperfections in an analysis is by imposing scaled linear bifurcation buckling modes as initial imperfections. [ECCS Technical Committee 8, 2008]. This method is used in the following in order to examine the influence of modes on the buckling load.

A case of imperfections modes of the tower are found with a horizontal load in the reference point. It is apparent, that these modes are of very local character and concentrated around relatively small sections of the tower. Two modes are chosen and presented in Figure 4.26 and 4.27. The selection of these modes is based on assessment of their possible influence on the limit buckling load of the tower. The chosen imperfection modes have bumps and dents in places, where stresses are concentrated during buckling analysis, and the modes are relatively different in nature.

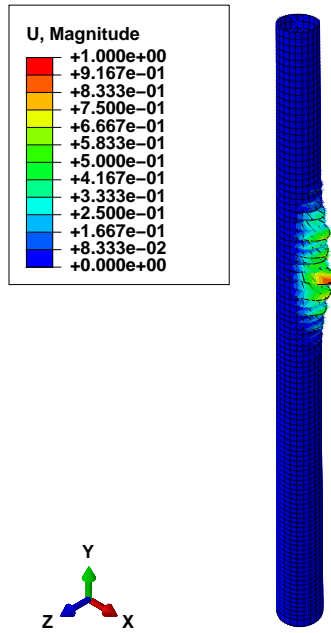


*Figure 4.26.* Mode shape 1, case 1.

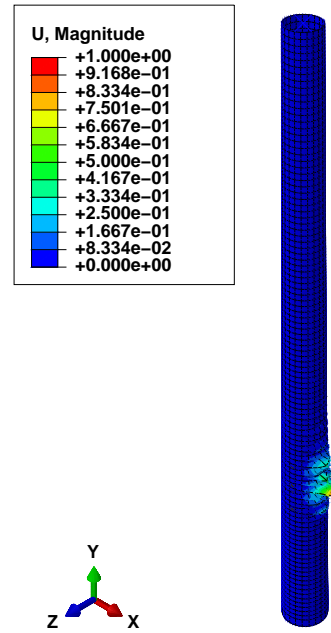


*Figure 4.27.* Mode shape 5, case 1.

It can be argued whether or not these imperfection modes with very local character are realistic to encounter in real turbine towers. Thus it is examined, if it is possible to obtain bifurcation buckling modes with a more global and realistic character. This is done by changing the varying wall thickness of the tower to a constant value and by changing load direction. Three additional cases of imperfections modes are found. An overview is seen in Table 4.2.

Case	Load direction	Wall thickness	Mode shape characteristics
1	→ (x direction)	Varying	Local
2	→ (x direction)	Constant	Local
3	↓ (-y direction)	Varying	Local
4	↓ (-y direction)	Constant	Global

*Table 4.2.* Load direction and assumptions of wall thickness in the four bifurcation buckling analysis. The constant wall thickness is set to 0.02m

It turns out that case 2 and 3 gives very similar mode shapes as in case 1. Modes are all of local character and limited to relatively small sections of the tower. Modes from case 2 and 3 are seen in Appendix D.

Completely different mode shapes with patterns of more global character are found with case number 4, where the tower with constant wall thickness is subjected to a compressive force. Two mode shapes from case 4 are presented in Figure 4.28 and 4.29.

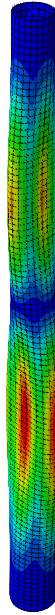
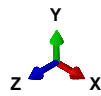
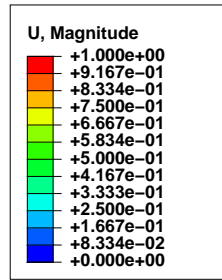


*Figure 4.28.* Mode shape 4, case 4.

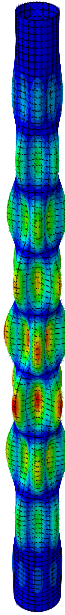
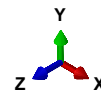
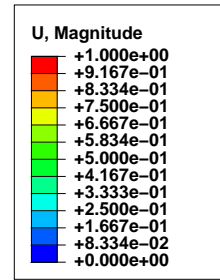


*Figure 4.29.* Mode shape 9, case 4.

Mode shape 1 and 5 from case 1, and mode shape 4 and 9 from case 4 are now applied as scaled initial imperfections in analysis with a static load and a time-varying impulse load. The mode shape vector is the eigenvector found in bifurcation buckling analysis, and contains relative displacements of nodes. The tower is modelled in such a way that mode shape factors correspond to the maximum deformation of imperfections in meters. It is chosen to introduce mode scaling factors between 0.01 and 0.1, which corresponds to maximum initial displacements between 1cm and 10cm. Imperfections of more than 10cm seem very unlikely and are causing problems with too initial distorted elements as well.

#### 4.5.1 Imperfection sensitivity analysis with static load

Mode shapes are extracted and applied as initial imperfections, and a horizontal point load is applied in the reference point (x-direction). Buckling loads are found to each scaled imperfection, and are normalized with the static buckling load of the perfect tower ( $4.4338 \cdot 10^3 \text{kN}$ ), see Figure 4.30.

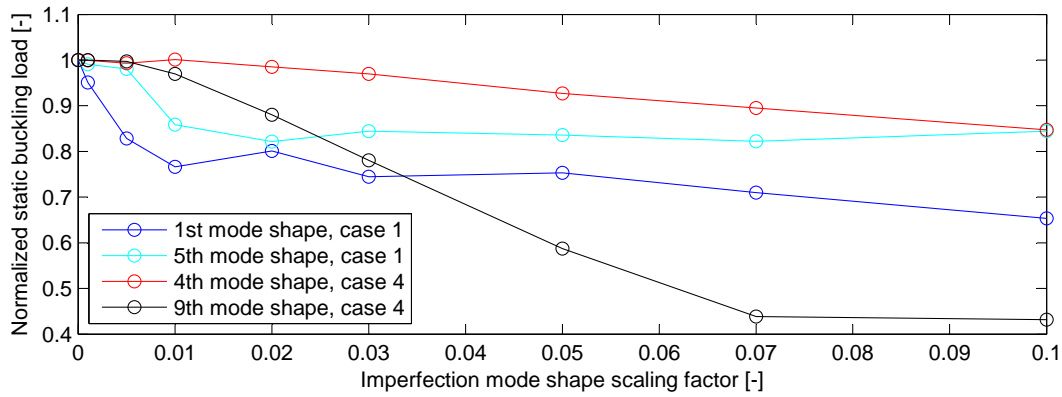


**Figure 4.30.** Influence of imperfections on static buckling loads.

It is clear, that the static buckling load decreases with the introduction of imperfections in general. It is however possible to obtain a normalized static buckling load greater than 1, when the 4th mode shape from case 4 is scaled by 0.01.

#### 4.5.2 Imperfection sensitivity analysis with impulse load

The load is applied in the reference point (x-direction) as an impulse load with various durations, see Figure 4.1(b). The magnitude of the load is equal to the static buckling load of the perfect structure (load ratio 1). Load duration,  $t_{impulse}$ , which causes buckling is found and normalized with the  $t_{impulse}$  at load ratio 1 without imperfections (0.73s). The normalized load durations to cause buckling as function of different scaled imperfections are seen in Figure 4.31.

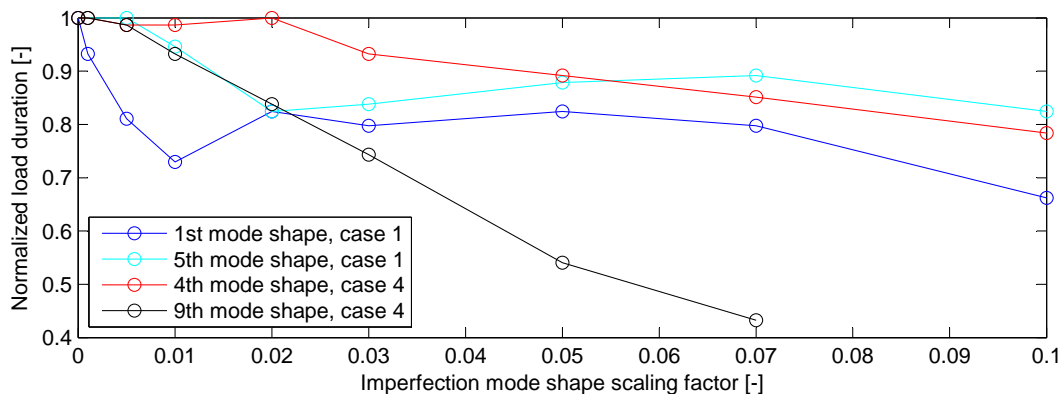


**Figure 4.31.** Imperfection sensitivity analysis with normalized load duration as function of scaled imperfection mode shape.

It is seen from Figure 4.31, that the load duration decreases as function of the imperfection scaling factor. The reduction in  $t_{impulse}$  is similar to the reduction of the buckling load in the static case. It should though be mentioned that because of no significant change in vertical acceleration or velocity of the reference point, it is not possible find the buckling point, when mode 9 (case 4) is scaled by more than 0.07.

Imperfection sensitivity analysis shows that imperfections have significant influence on the structural response in both static and dynamic analysis. The choice of imperfection shape is essential for the reduction in buckling load. Results from the four applied imperfections shows, that there is large variation in the reduction of buckling load and load duration between each imperfection shape.



## CHAPTER 5

---

# Analysis with Combined Time-varying Wind Loads

---

Previous chapters examined the structural response of the wind turbine tower with a simple lateral load. When a wind turbine is subjected to real wind loads, forces and moments along and around all axes of the tower will be generated. This chapter examines the effects of combining multiple loads and how a wind load varies over time.

Wind loads on a wind turbine are a comprehensive study, and a thorough examination and determination of so are beyond the scope of this thesis and will not be covered. It is instead chosen to extract wind generated loads from the software FAST (Fatigue, Aerodynamics, Structures, and Turbulence).

Before application of these wind generated loads, this chapter is initiated with an analysis of simpler load combinations. This is done in order to clarify the influence of gravitational forces and the combination of multiple loads acting simultaneously.

### 5.1 Simple load combinations

Past results are all obtained by omitting gravitational forces, which are now included in the model. Figure 5.1 shows the relation between force  $F_x$  and moment  $M_z$ , that causes buckling in a static analysis. The two loads are acting in the reference point as before, see Figure 5.2.

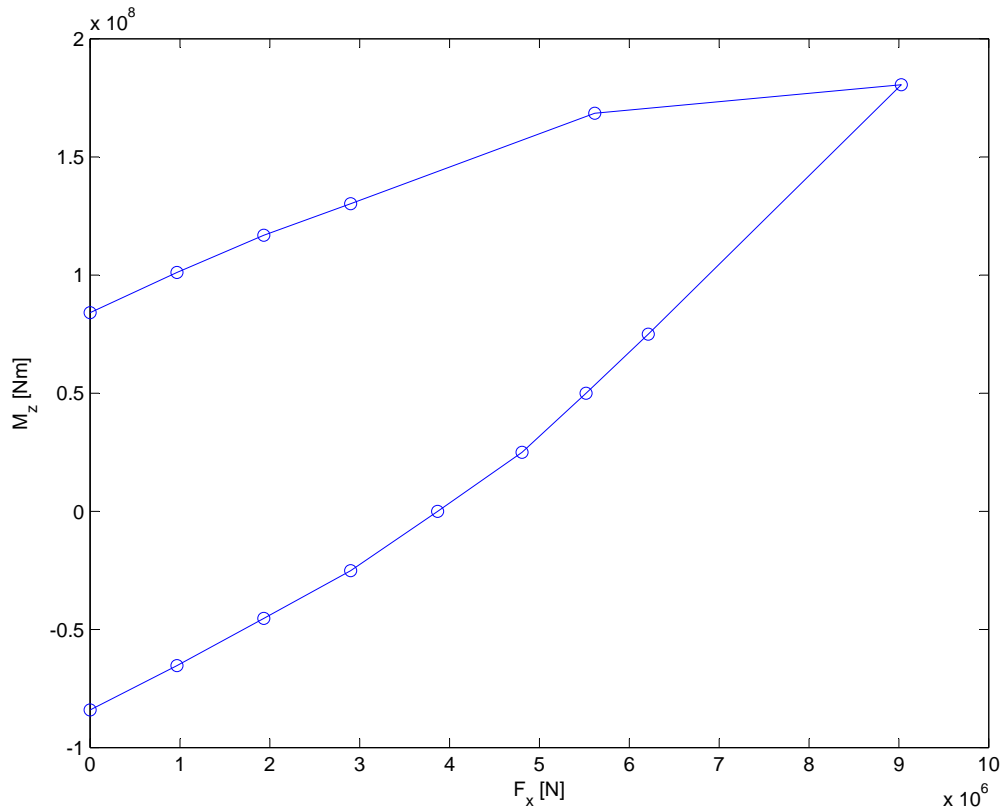


**Figure 5.1.** Relation between  $F_x$  and  $M_z$ .

Figure 5.1 shows, that a negative moment reduces the applicable force, and that a positive moment will increase the required force to cause buckling. Three combinations of lateral force  $F_x$  and moment  $M_z$  are presented in Table 5.1. All combinations include gravity, and each combination of load causes buckling of the tower in a static analysis.

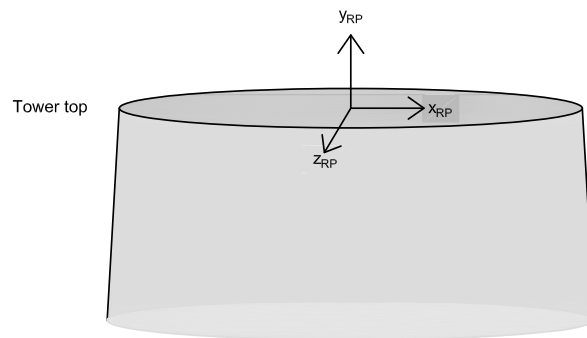


**Figure 5.2.** Local coordinate system at reference point.

	$F_x$ [kN]	$M_z$ [kNm]
Load combination 1	$3.867 \cdot 10^3$	0
Load combination 2	$1.934 \cdot 10^3$	$-45.321 \cdot 10^3$
Load combination 3	0	$-84.078 \cdot 10^3$

**Table 5.1.** Load combinations consisting of static buckling loads with gravity included.

Notice that  $M_z$  is with negative sign, since that will deform the tower in the positive x-direction. Load combination 1 shows, that the introduction of gravity reduces the static buckling load, which earlier was found to  $4.4338 \cdot 10^3 \text{ kN}$ . The three load combinations are applied as impulse loads in a dynamic analysis with various durations,  $t_{impulse}$ , and the corresponding load combination ratio is found. The relation between  $t_{impulse}$  and load combination ratio is illustrated in Figure 5.3.

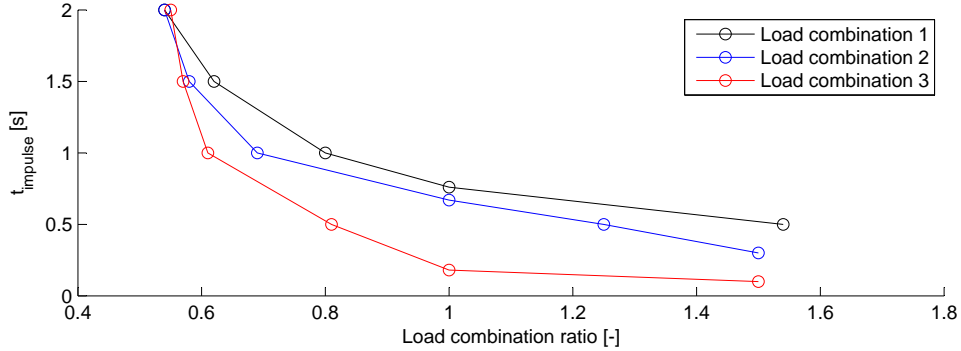


**Figure 5.3.**  $t_{impulse}$  as function of load factor with three load combinations.

The figure shows that all load combinations have similar relations between  $t_{impulse}$  and load factor, and that moments in general needs shorter durations to cause buckling. I.e. lower load combination ratio gives higher load durations, independent of load combination.

## 5.2 Wind generated loads

The software FAST can be used to perform aeroelastic simulations to predict loads on a wind turbine. As input to FAST is it chosen to simulate a random generated wind field orthogonal to the rotor of a 5MW reference turbine, with a statistical distribution and a mean wind speed of 50 m/s, see Figure 5.4. The wind turbine is no longer operating in this extreme wind condition, and any harmonic motions from rotating parts vanish.

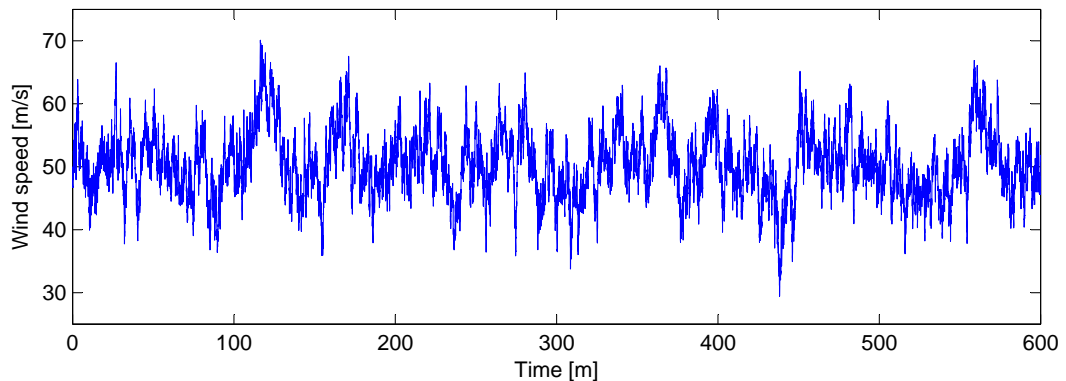


**Figure 5.4.** Random generated wind field acting orthogonal on the rotor.

Section forces and moments can be extracted at different positions on the model. It is

chosen to extract forces and moments at the low-speed shaft, see Figure 5.5. This is done to avoid as many unpredictable inertia effects as possible and these forces and moments can be applied relatively simple without changing properties of the finite element model. The normal and shear forces  $F_{x_s}$ ,  $F_{y_s}$ , and  $F_{z_s}$  are constant along the  $x_s$  axis. The extracted moments are located at the rotor apex and are named  $M_{x_s}$ ,  $M_{y_s}$  and  $M_{z_s}$ .

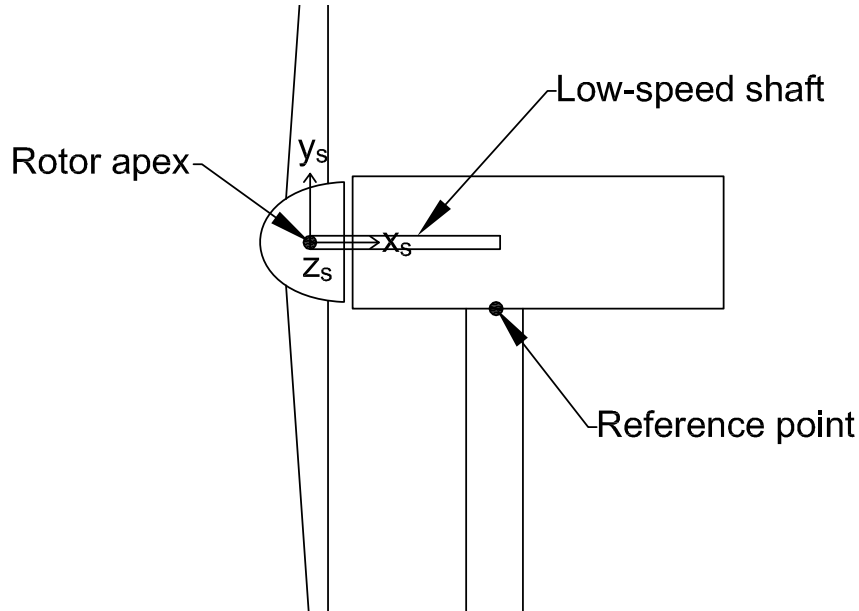


**Figure 5.5.** Location of low-speed shaft.

The shaft is tilted  $5^\circ$  in the reference wind turbine model as illustrated by the dashed lines in Figure 5.6. Extracted forces and moments are projected onto the  $x_s, y_s, z_s$  coordinate system in order to take the tilt into account.

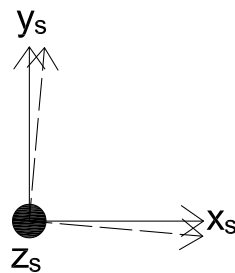


**Figure 5.6.** Rotation of the shaft-coordinate system.

It is chosen to move the forces and moments acting on the  $x_s, y_s, z_s$ -coordinate system (Figure 5.6) to the  $x_{RP}, y_{RP}, z_{RP}$ -coordinate system directly without changing any of their magnitudes. The RP-coordinate system is seen in Figure 5.2.

Each simulated wind field has a duration of 10 minutes, which gives the time variation of forces and moments in 10 minutes. A simulation is performed, where the 10 minutes time-series of the six loads are applied to the tower. This is done, since it is unclear how the combination of the six forces affects the response. Results shows that the greatest horizontal displacements of the reference point is in the order of 0.4-0.5m, which is far

from the deformation just before buckling (3.082m), when only the horizontal buckling load  $P = 4.4338 \cdot 10^3 \text{kN}$  is applied. This indicates that buckling probably not was a determining factor in the structural design. Minimum, maximum, and mean values of forces and moments are listed in Table 5.2.

	Minimum value	Maximum value	Mean
$F_x$ (Fore-Aft)	86.7kN	<b><u>268.3kN</u></b>	172.6kN
$F_y$ (Up-Down)	<b><u>-1076.1kN</u></b>	-721.2kN	-898.7kN
$F_z$ (Side-to-Side)	<b><u>-198.1kN</u></b>	166.1kN	-2.16kN
$M_x$ (Bending Side-to-Side)	<b><u>-1305.9kNm</u></b>	1128.6kNm	2.24kNm
$M_y$ (Torsion)	-1789.7kNm	<b><u>1993.7kNm</u></b>	203.7kNm
$M_z$ (Bending Fore-Aft)	<b><u>-1363.7kNm</u></b>	1498.8kNm	200.7kNm

**Table 5.2.** Forces and moments generated by generated wind field.

The assumed worst combination of loads is highlighted with an underline. There is great variation over time in the three forces and three moments, and none of the extreme values are present simultaneously. This is seen on their time series, which can be found in Appendix E. Figure 5.7 shows the load variation over 60 representative seconds of the entire time series.

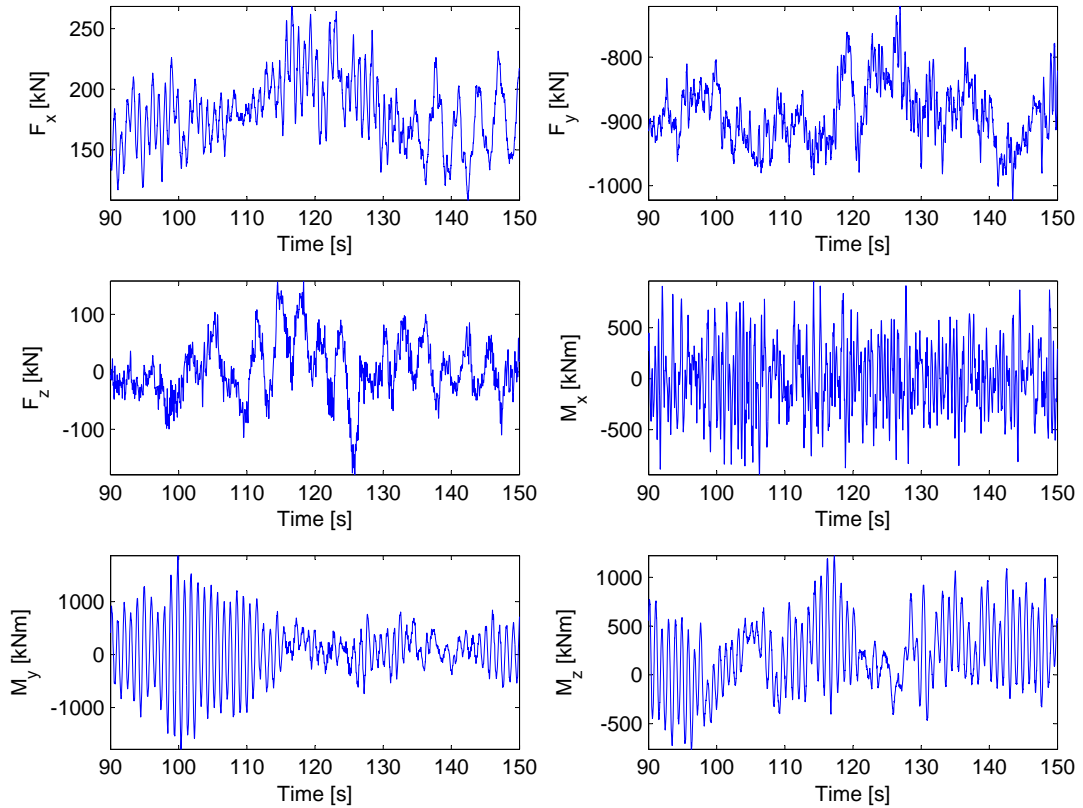


**Figure 5.7.** Sections of all loads series.

The peak value of  $F_x$  occurs after 116.6s, and it can be seen that none of the other forces assumes their peaks values at that time. It is investigated if any relationship exists between the variations of loads in the data. It is not possible to obtain such a relation between

loads, and one peak load does not exclude the presence of another peak load.

It is assumed, that the highlighted peak values listed in Table 5.2 occurs simultaneously, and that the tower is designed using this combination. This combination must be factorized by 7.63 in order to cause buckling in a static analysis. The magnitude of this factor confirms earlier findings, where it was found that buckling probably not determines the structural design, or that extreme wind situations are not used as governing design case. The factor would be significantly smaller if imperfections and safety factors are included in the model.

Since  $F_y$  only contains gravitational forces from the rotor, it is replaced by applying gravity to the whole model. The magnified static buckling load combination is seen in Table 5.3.

Load	Value
$F_x$ (Fore-Aft)	$2.046 \cdot 10^3 \text{ kN}$
$F_z$ (Side-to-Side)	$-1.511 \cdot 10^3 \text{ kN}$
$M_x$ (Bending Side-to-Side)	$-9.957 \cdot 10^3 \text{ kNm}$
$M_y$ (Torsion)	$15.202 \cdot 10^3 \text{ kNm}$
$M_z$ (Bending Fore-Aft)	$-10.398 \cdot 10^3 \text{ kNm}$

**Table 5.3.** Static buckling load combination.  $F_y$  is replaced by applying gravity to the whole model. The loads are the highlighted values in Table 5.2 (with the exception of  $F_y$ ), multiplied by a factor of 7.63.

### Duration of peak values

Durations of peak values in the data are very short, and it should be mentioned that the moments and  $F_z$  varies from positive to negative values within a second. It is now examined, how the mean values of the peaks decreases with the width of the peak. The examination is carried out by "scanning" the entire time series of each load with time intervals spanning from 0 to 2.5s. The mean value of the load in each interval is found. The worst (maximum or minimum dependent on the load type) values of these means are then normalized with the peak value in the load series. The assumed worst peak values from Table 5.2 (underlined) are used in the normalization.

Examples of this method this is illustrated in Figure 5.8 and 5.9.

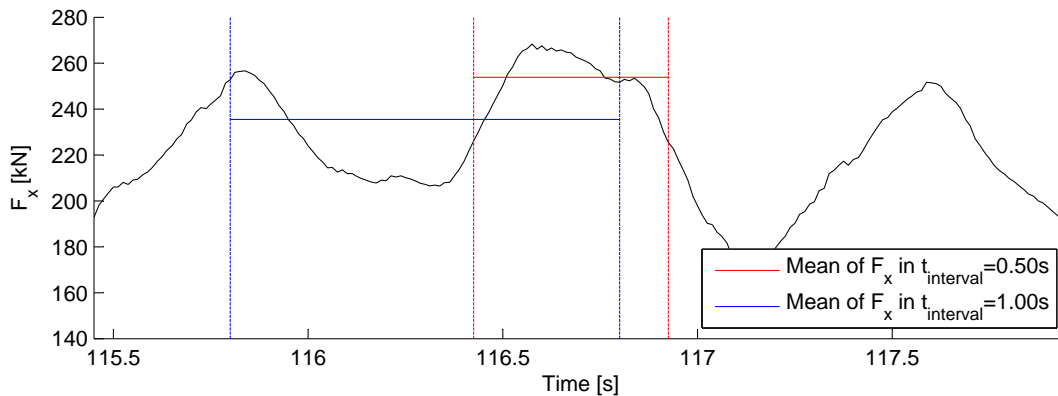


**Figure 5.8.**  $F_x$  as function of time with an illustration of mean values in time intervals.

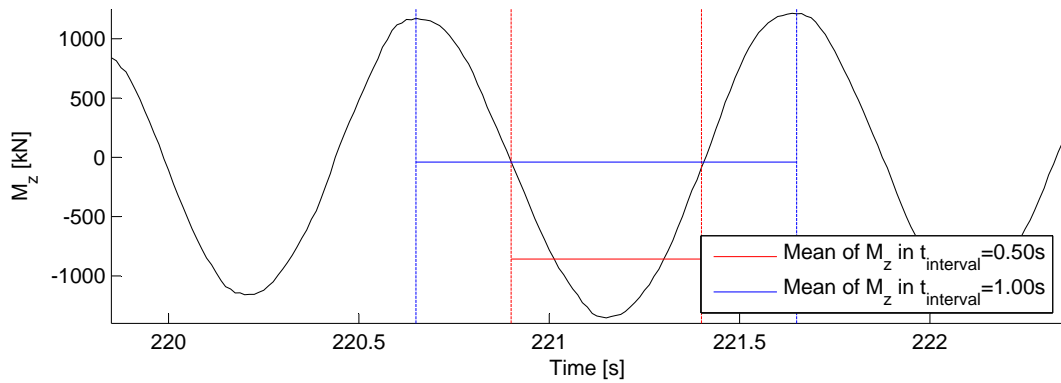


**Figure 5.9.**  $M_z$  as function of time with an illustration of mean values in timeintervals.

Results for all loads are presented in Figure 5.10. Results are expressed in terms of size of time interval as function of ratio between maximum mean in interval and the peak value for each of the three forces and three moments.

The considered time interval is up to 2.5s, and as seen Figure 5.8 and 5.9, more than one peak contributes to the mean value in the higher intervals. This can also be seen by the jumps in some of the graphs in Figure 5.10.

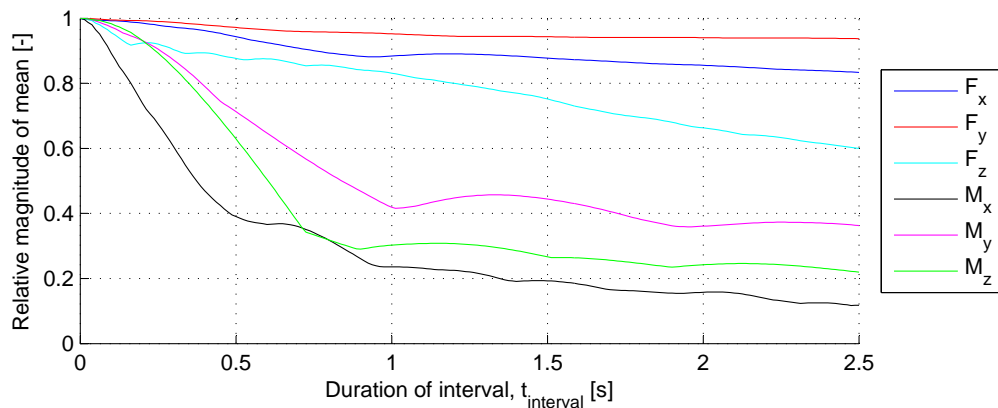


**Figure 5.10.** Relation between time interval size and magnitude of load for different loads.

10 load combinations are made and listed in Table 5.4. Each combination consists of the highest mean values of each load to the corresponding time interval. By making these combinations it is again assumed, that all loads are acting simultaneously in each combination.

Load combination	$t_{interval}$ [s]	$F_x$	$F_y$	$F_z$	$M_x$	$M_y$	$M_z$	$t_{impulse}$ [s]
1	0.25	0.98	-	0.92	0.67	0.90	0.89	1.13
2	0.50	0.94	-	0.88	0.39	0.71	0.63	1.23
3	0.75	0.90	-	0.86	0.34	0.55	0.33	1.38
4	1.00	0.88	-	0.83	0.24	0.42	0.30	1.48
5	1.25	0.89	-	0.79	0.22	0.45	0.30	1.47
6	1.50	0.88	-	0.75	0.19	0.44	0.27	1.58
7	1.75	0.87	-	0.70	0.16	0.39	0.25	1.73
8	2.00	0.86	-	0.66	0.16	0.36	0.24	1.88
9	2.25	0.84	-	0.63	0.13	0.37	0.24	1.98
10	2.50	0.83	-	0.60	0.12	0.36	0.22	2.17

**Table 5.4.** Relative load magnitude of load combinations.

Relative load magnitudes in each combination are multiplied with the static buckling loads in Table 5.3. Combinations are then applied in a dynamic analysis as impulse loads with duration equal to  $t_{interval}$ . This is done to investigate the relation between durations and load magnitudes. Results are presented in terms of the amount of strain energy the load combination accumulates in the tower.

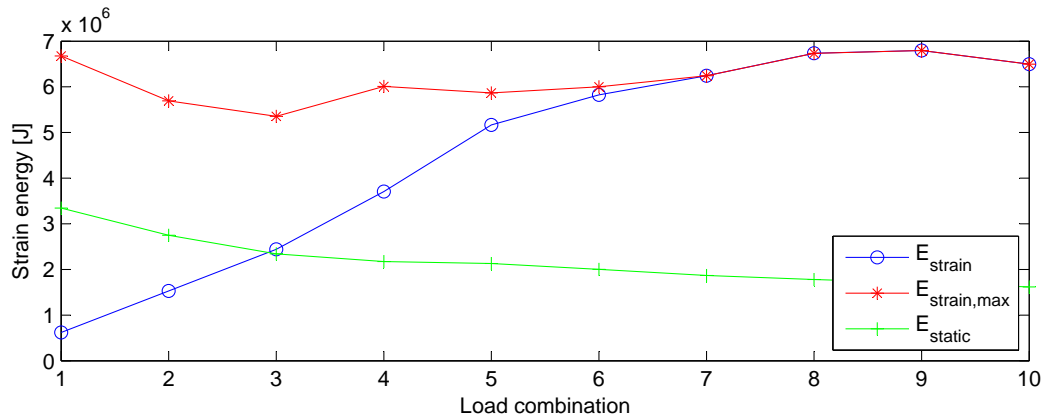


**Figure 5.11.** Strain energy to each load combination.

The red line indicates the necessary strain energy to cause buckling for the given load combination. This energy level is obtained by increasing the load duration of each load combination until buckling occurs. The buckling load duration  $t_{impulse}$  to each load combination are seen in Table 5.4. It is apparent, that load combination 7 to 10 will induce buckling of the tower, since their corresponding time interval exceeds  $t_{impulse}$ , see Figure 5.12. Load durations about half the natural period of the tower are causing the greatest amount of strain energy, which is consistent with earlier findings.

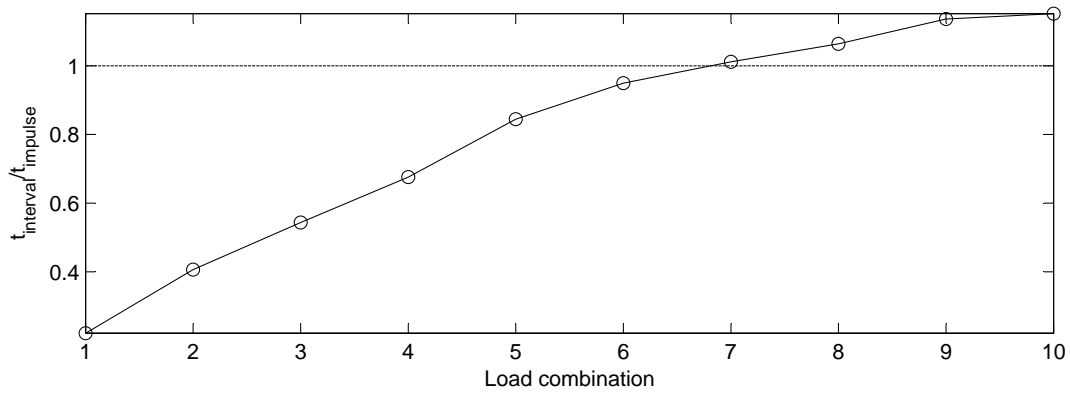


**Figure 5.12.** Ratio between  $t_{interval}$  and  $t_{impulse}$  at each load combination.  $t_{interval}$  causes buckling, when the ratio is 1 or above.

The load combinations are also applied in a static analysis, and their strain energy level are illustrated with the green line in 5.11. The static analysis induces highest strain energy in load combination 1 and 2, while the dynamic analysis of load combination 3 to 10 causes highest strain energy. This means, that a static analysis with load combination 3 to 10 underestimates the deformations. Where the green and blue graphs intercept is where static analysis changes from overestimating to underestimating the deformations.



## CHAPTER 6

---

# Conclusion

---

The influence of time-varying loads on the structural behaviour of a wind turbine tower is clarified and depicted throughout this thesis. Numerous studies are showing, how it is possible to compare static and time-varying loads, and which parameters that must be taken into account during simplification of loads with time dependency.

Effects of time-variance of loads are examined with a preliminary parameter study of limit load buckling behaviour of a simple truss. It can be concluded, that the magnitude of an impulse load, which causes limit load buckling, is dependent on the load duration. Smaller load (relative to the static buckling load) can be applied for a longer time and vice versa. It is also found, that a harmonic load results in a dynamic amplification if the load period coincides with the natural period of the truss. A higher dynamic amplification is present if the load period is slightly larger than the natural period due to the deformation dependent structural stiffness.

The parameter study is used as background knowledge for further studies of a full size finite element modelled wind turbine tower. The two structures are very different in nature but exhibits common structural features.

Effects of time-varying loads on the tower are similar to preliminary findings, and it is found, that the relation between impulse load duration and magnitude can be explained by kinetic and potential strain energy in the system. A similar structural response is observed with an inclusion of a linear viscous damping model. It can be concluded, that initial imperfections have a great influence on the tower response, and that the load bearing capacity decreases with increasing magnitude of imperfections.

The studies with relative simple load scenarios are expanded with analysis of real wind generated loads. It is apparent, that the combination of wind loads with different orientation and duration complicates the interpretation of results, and the structural response cannot be directly compared with former results with simple loads. The assumed worst combination of loads is applied instead, and it is assumed that these loads have peak values simultaneously. It can be concluded, that combinations of loads and load durations relates in the same manner for different load combinations. The amount of strain energy in the tower reaches maximum values, when the duration of the wind load peaks approaches half the natural period of the tower. This finding is again based on the assumption that different load peaks appear at the same time.

It can finally be concluded that combinations of wind loads averaged over short durations applied statically induces larger deformations than the same load combinations applied dynamically. It is also found that load combinations with loads averaged over longer durations induce larger deformations in the dynamic analysis. The point where deformations of the tower cannot be adequately described by static analysis is dependent of the load time-series and structural properties. Peak values of time-varying loads can be used to define the buckling load in a stability analysis of a wind turbine tower. But the variation of the time-varying loads and the duration of each peak are of essential importance and must be considered. Longer duration - smaller load. Especially if load durations approach values which coincide with half the natural period of the tower.

---

# Bibliography

---

- Alipour and Zareian, 2008.** A. Alipour and F. Zareian. *Study Rayleigh Damping in Structures: Uncertainties and Treatments*. URL: [http://www.iitk.ac.in/nicee/wcee/article/14\\_14-0243.PDF](http://www.iitk.ac.in/nicee/wcee/article/14_14-0243.PDF), 2008. Downloaded: 05-26-2014.
- Almroth and Brogan, 1972.** B.O Almroth and F.A. Brogan. *Bifurcation buckling as an Approximation of the Collapse Load for General Shells*. AIAA Journal, 1972.
- Brome, 2010.** Trent Brome. *Wyoming turbine collapse*. URL: <http://www.windaction.org/posts/29881-wyoming-turbine-collapse#.Uz1xY6j1auJ>, 2010. Downloaded: 03-31-2014.
- Bushnell, 1989.** D. Bushnell. *Computerized buckling analysis of shells*. ISBN: 90-247-3099-6. Kluwer Academic Publishers, 1989.
- Castro, Zimmermann, Arbelo, Khakimova, Hilburger, and Degenhardt, 2013.** Saullo G.P. Castro, Rolf Zimmermann, Mariano A. Arbelo, Regina Khakimova, Mark W. Hilburger, and Richard Degenhardt. *Geometric imperfections and lower-bound methods used to calculate knock-down factors for axially compressed composite cylindrical shells*. Elsevier, 2013.
- Cook, Malkus, Plesha, and Witt, 2001.** Robert D. Cook, David S. Malkus, Michael E. Plesha, and Robert J. Witt. *Concepts and Applications of Finite Element Analysis*. ISBN: 978-0-471-35605-9, 4th edition. John Wiley & Sons Inc., 2001.
- DS/EN 1990, 2007.** DS/EN 1990. *Eurocode - Basis of structural design*, 2007.
- ECCS Technical Committee 8, 2008.** ECCS Technical Committee 8. *Structural Stability - Buckling of Steel Shells European Design Recommendations*. ISBN: 92-9147-000-92, 5th edition. ECCS, 2008.
- Jonkman, Butterfield, Musial, and Scott, 2009.** J. Jonkman, S. Butterfield, W. Musial, and G. Scott. *Definition of a 5-MW Reference Wind Turbine for Offshore System Development*. National Renewable Energy Laboratory, 2009.
- Krenk, 2009.** Steen Krenk. *Non-linear Modeling and Analysis of Solids and Structures*. ISBN: 978-0-521-83054-6. Cambridge University Press, 2009.

**Nielsen, Stærdahl, and Andersen, 2007.** Søren R.K. Nielsen, Jesper W. Stærdahl, and Lars Andersen. *Plate and Shell Theory*. Aalborg University - Department of Civil Engineering, 2007.

**Ottosen and Ristinmaa, 2005.** Niels Saabye Ottosen and Matti Ristinmaa. *The Mechanics of Constitutive modeling*. ISBN: 978-0-080-44606-6. Elsevier Science, 2005.

**Sahu, Hiloidhari, and Baruah, 2013.** Bikash Kumar Sahu, Moonmoon Hiloidhari, and D.C. Baruah. *Global trend in wind power with special focus on the top five wind power producing countries*. URL: <http://www.sciencedirect.com/science/article/pii/S1364032112006399>, 2013. Downloaded: 03-26-2014.

**Schmidt, 2000.** Herbert Schmidt. *Stability of steel shell structures - General Report*. ISBN: 978-0-471-35605-9. Department of Civil Engineering, University of Essen, 2000.

**Simulia, 2011.** Simulia. *Abaqus Theory Manual 6.11*. Simulia, 2011.

**Vestas Wind Systems A/S, 2014.** Vestas Wind Systems A/S. *World's most powerful wind turbine now operational*. URL: <http://vestas.com/en/media/~media/eaf56b4c49964c8faf5f550ad0b1dec0.ashx>, 2014. Downloaded: 05-22-2014.

**Williams and Todd, 2000.** M. S. Williams and J. D. Todd. *Structures - Theory and analysis*. ISBN: 978-0-333-67760-5. Palgrave Macmillan, 2000.

## APPENDIX A

---

### Simple model

---

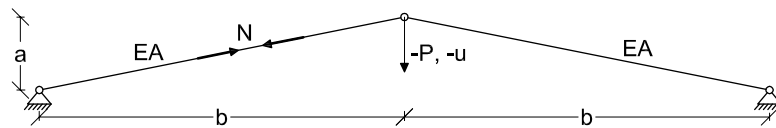


*Figure A.1.* Simply supported non-linear truss with two bar elements. A downward load is applied in the middle node.

- Cross sectional area,  $A = 0.01m^2$
- Young's modulus,  $E = 200 \cdot 10^9 Pa$
- Natural eigenfrequency:

$$\omega_0 = \sqrt{\frac{k}{m}}$$
$$k = \frac{EA}{l_0} \cdot 2 \cdot \left(\frac{a}{l_0}\right)^2$$



## APPENDIX B

---

### Tower properties

---

#### B.1 Tower dimensions

Height [m]	Radius (centerline) [m]	Wall thickness [m]
61.80	1.619	0.02
59.52	1.637	0.016
56.66	1.663	0.016
53.80	1.690	0.016
50.95	1.716	0.014
48.10	1.742	0.014
45.25	1.768	0.015
42.40	1.794	0.016
39.55	1.820	0.017
36.70	1.846	0.018
33.85	1.872	0.019
31.01	1.898	0.020
28.16	1.924	0.021
25.32	1.950	0.021
22.31	1.984	0.022
19.50	2.018	0.022
16.69	2.052	0.023
13.88	2.085	0.024
11.07	2.119	0.024
8.27	2.153	0.025
5.47	2.186	0.038
3.67	2.208	0.050
0.87	2.241	0.038
0.13	2.250	0.038

*Table B.1.* Measures of wind turbine tower.



## APPENDIX C

---

# Nonlinear iteration methods

---

Numerical iteration schemes and their pros and cons are presented in the following.

### C.1 Newton-Rhapson method

A commonly used method to generate a load-displacement curve for a nonlinear problem is the Newton-Raphson method. This method uses the tangent stiffness to find the displacement for a given load step. In each load step several iterations are made, in which the tangent stiffness is updated according to the current displacement. This procedure is repeated until the residual between the external and internal force is sufficiently small. The following describes the properties of the Newton-Raphson scheme:

- Works well in both loading and unloading
- Fast convergence
- Problems can occur close to peak points
- Every iteration is computationally costly

[Ottosen and Ristinmaa, 2005]

The iterations for a single DOF problem is illustrated to the left in figure C.1.

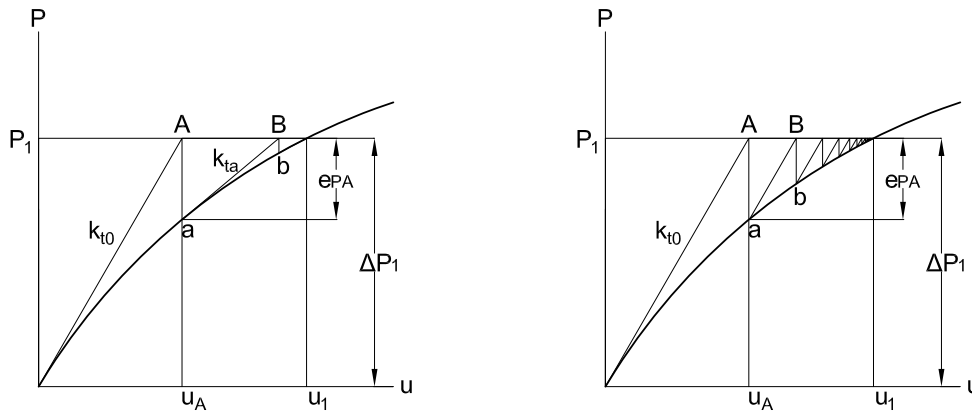


*Figure C.1.* Iterations to load level  $P_1$ . To the left is the Newton Raphson scheme and to the right is the modified Newton Raphson scheme.

## C.2 Modified Newton-Raphson method

Another iteration scheme very similar to the Newton-Raphson method is the modified Newton-Raphson method, which is illustrated to the right in figure C.1. Instead of generating a new stiffness in each iteration, this method only updates the stiffness after every load step. This leads to less computation time for each displacement increment, but on the other hand it might need more increments. So in some cases this method could be more efficient than the original method. The properties for the modified method are listed below.

- Converges slowly
- Every iteration is cheap

[Ottosen and Ristinmaa, 2005]

## C.3 Arc-length method

Both the Newton Raphson and the modified Newton Raphson method have problems converging to the load versus displacement curve, when the tangent stiffness is zero. This can be helped by generating the curve using displacement control or by the arc-length method. The arc-length can be used to describe complicated load versus displacement curves such as post-buckling. The main difference from the Newton Raphson methods is, that the arc-length method is controlled by a arc in each load step, this is illustrated in Figure C.2.

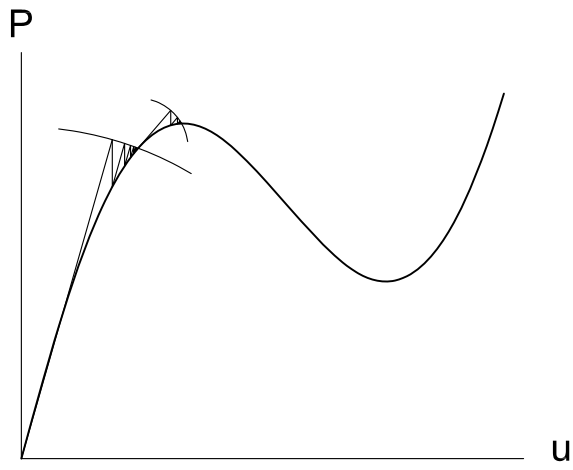


*Figure C.2.* Illustration of the arc-length method.



# APPENDIX D

## Imperfection mode shapes

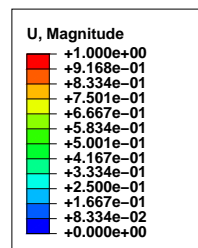


Figure D.1. Mode shape 4, case 2.

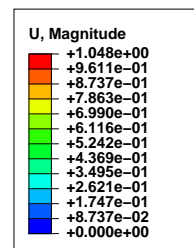


Figure D.2. Mode shape 10, case 2.

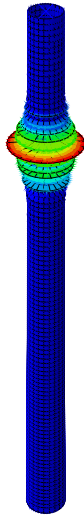
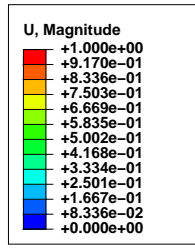


Figure D.3. Mode shape 3, case 3.

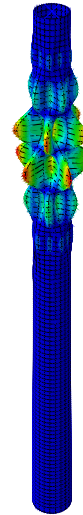
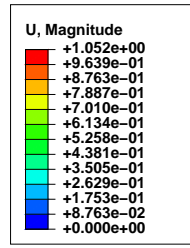


Figure D.4. Mode shape 15, case 3.

## APPENDIX E

---

### Wind generated loads

---

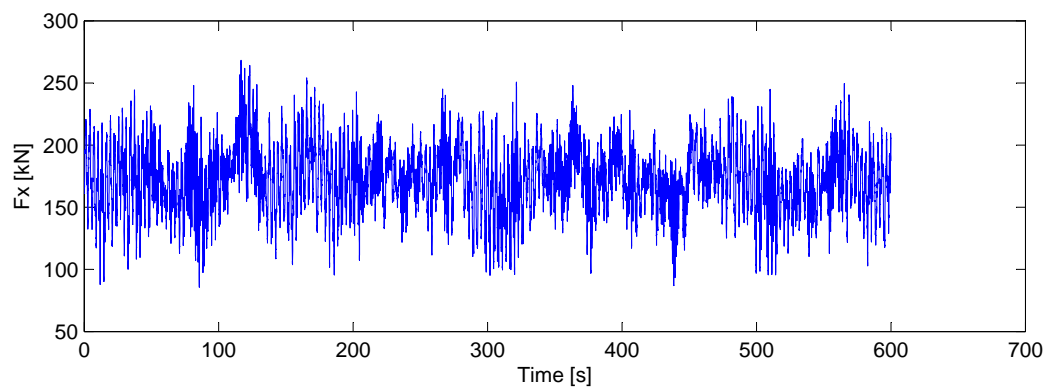


*Figure E.1.* Forces in force-aft direction.

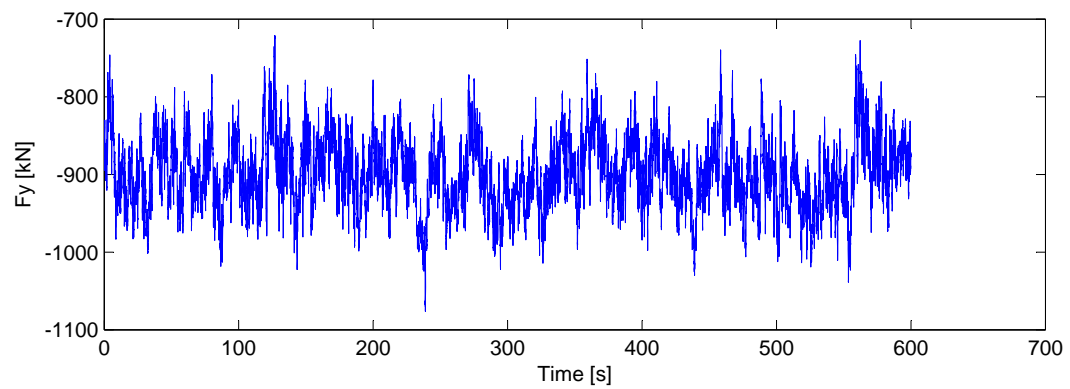


*Figure E.2.* Vertical force.

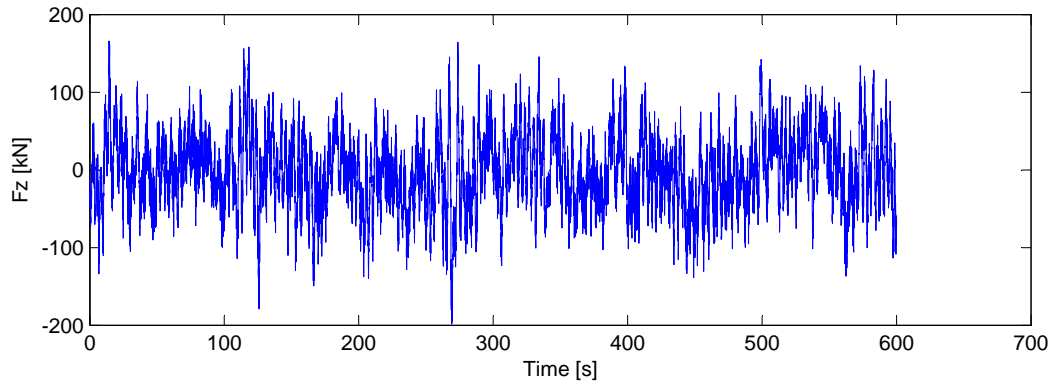


*Figure E.3.* Force from side-to-side.

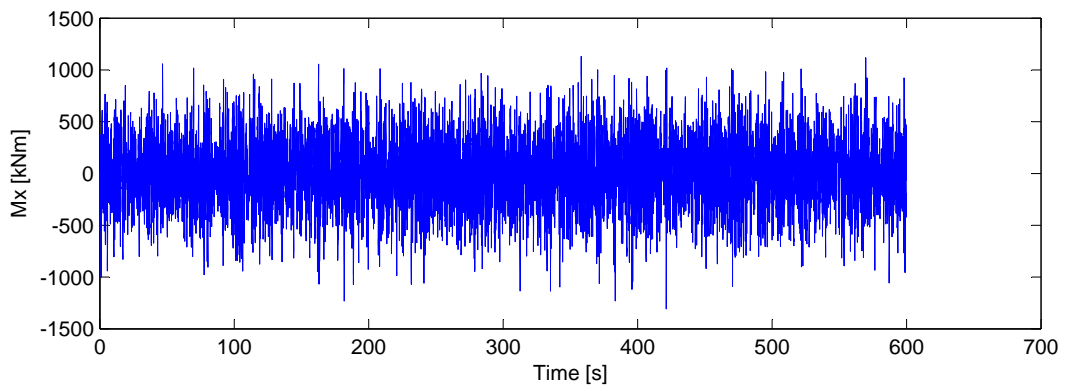


*Figure E.4.* Bending moment side-to-side.

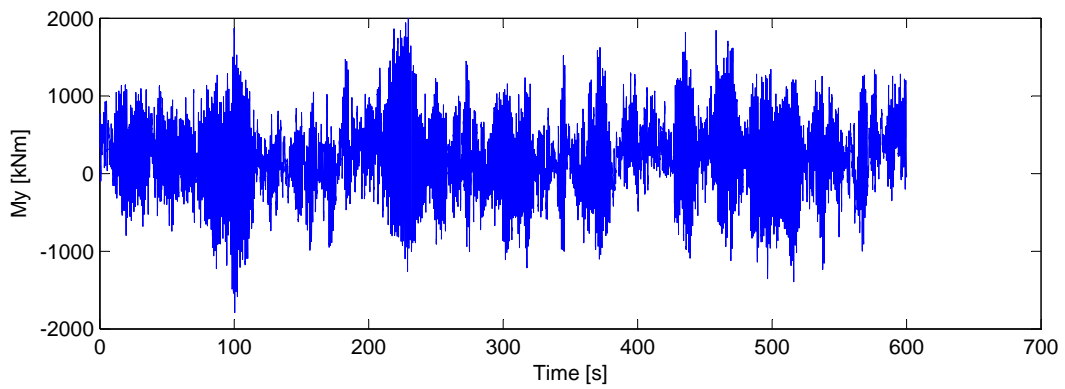


*Figure E.5.* Torsional moment.

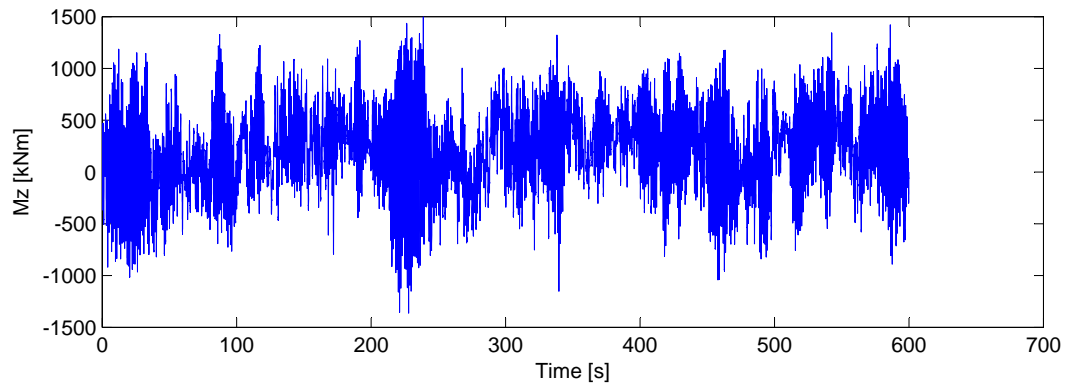


*Figure E.6.* Bending moment fore-aft direction.

## Projektplan for kort afgangprojekt (4. semester, MSc)

**Projektets titel:**

[angives på dansk og engelsk]

Ikke-lineær numerisk analyse af dynamisk lastet vindmølletårne

Nonlinear numerical analysis of dynamically loaded wind turbine towers

**Studieretning:**

B10K

**Studerende:**

Rasmus Bøgelund Madsen

Christian Munk Svendsen

**Studienr.:**

20093323

20093319

**Afleveringsform og sprog:**

[f.eks. rapport, artikel, poster eller website etc. på dansk eller engelsk]

Thesis in English

**Beskrivelse af projektet:**

[et kort abstract om projektets indhold, ca. 200 ord]

Many wind turbines throughout the world are designed and manufactured, based on requirements prescribed in international wind turbine standards. The thesis will examine whether or not simplified loads and durations, are adequate when designing wind turbine towers (cylindrical and conical tubes), and to which extent they may be conservative (or not). Different dynamic loads are simulated, and responses and behaviour of the tower is analysed and examined with non-linear finite element calculations.

In order to identify phenomena associated with a slender and thin-walled structure undergoing dynamic loading, a simple 2D structure is first modelled and analysed. Focus is the coupling between dynamics and instability (buckling) related to short-term cyclic or pulse-like loads. Observations and findings from this study shall then provide a basis for the more complex 3D analysis.

**Goals:**

- To gain knowledge about stability problems and failure mechanisms associated with thin-walled shell structures.
- The ability to apply correct terminology and methods within the field of instability problems and non-linear dynamic finite element calculations.
- The ability to create a finite-element model for dynamic analysis including nonlinear response.
- The ability to synthesise and discuss problems and limitations which may arise from used methods.
- The ability to interpret and discuss obtained results.

**Tidsplan:**

01/02 - 2014: Thesis start

01/03 - 2014: Literature study

15/03 - 2014: Analysis of simple model

- Clarify the snap-through problem

- Influence of inertia forces and stiffness on structural response

01/04 - 2014: Numerical modelling of tower

01/06 - 2014: Analysis of tower  
10/06 - 2014: Submission of thesis

**Vejledere:**

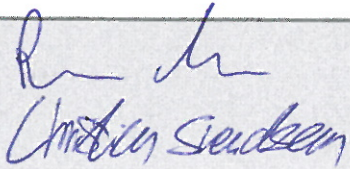
Søren Madsen

Lars Vabbersgaard Andersen

**Studerende:**

Dato: 28/2-2014

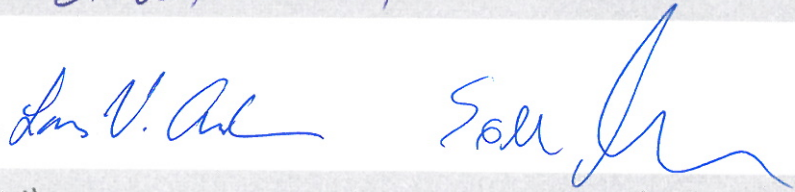
Underskrift(er):



**Hovedvejleder:**

Dato: 28/2-2014

Underskrift:



**Virksomhed eller institution (hvis relevant):**

Dato:

Underskrift:

**Studieleder:**

Dato:

17/3-14

Underskrift:



**Bemærk:**

- Blanketten udfyldes af den studerende i samarbejde med vejleder
- Blanketten skal være underskrevet af studerende, vejleder og evt. virksomhed inden aflevering til studienævnet
- Den underskrevne blanket sendes til godkendelse (med intern post eller mail) til din studienævnsekretær